Article

Immunity

Distinct Foxp3 enhancer elements coordinate development, maintenance, and function of regulatory T cells

Graphical abstract

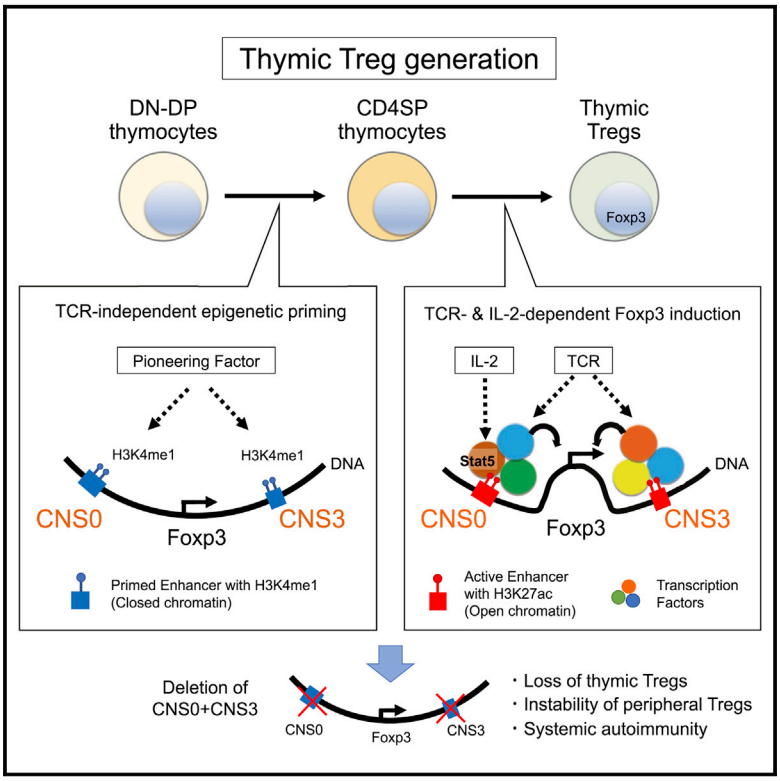

Highlights

- Enhancers activated at Foxp3-CNS0 and -CNS3 are indispensable for thymic Treg generation
- CNS0 and CNS3 interact with other enhancers and Foxp3 promoter during Treg development
- Deletion of both CNS0 and CNS3 causes lethal autoimmunity
- CNS0 is responsible for IL-2-dependent induction and maintenance of Foxp3 expression.

Authors

Ryoji Kawakami, Yohko Kitagawa, Kelvin Y. Chen, ..., Keiji Hirota, Naganari Ohkura, Shimon Sakaguchi

Correspondence

shimon@ifrec.osaka-u.ac.jp

In brief

The Foxp3^{+} Treg generation process in the thymus has not been fully understood, especially in the perspective of genomic enhancer coordination. Kawakami et al. reveal that two independently activated enhancers, Foxp3-CNS0 and Foxp3-CNS3, cooperatively induce and maintain Foxp3 expression for the establishment of self-tolerance.

Kawakami et al., 2021, Immunity *54*, 947–961
May 11, 2021
https://doi.org/10.1016/j.immuni.2021.04.005

CellPress

Immunity

CellPress

Article

Distinct Foxp3 enhancer elements coordinate development, maintenance, and function of regulatory T cells

Ryoji Kawakami,[1,2,5] Yohko Kitagawa,[1,2,5] Kelvin Y. Chen,[1] Masaya Arai,[1] Daiya Ohara,[3] Yamami Nakamura,[1] Keiko Yasuda,[1,2] Motonao Osaki,[1,2] Norihisa Mikami,[1,2] Caleb A. Lareau,[4] Hitomi Watanabe,[3] Gen Kondoh,[3] Keiji Hirota,[3] Naganari Ohkura,[1] and Shimon Sakaguchi[1,2,6,*]

[1]Department of Experimental Immunology, Immunology Frontier Research Center, Osaka University, Osaka 565-0871, Japan
[2]Department of Experimental Pathology, Institute for Frontier Life and Medical Sciences, Kyoto University, Kyoto 606-8507, Japan
[3]Laboratory of Integrative Biological Science, Institute for Frontier Life and Medical Sciences, Kyoto University, Kyoto 606-8507, Japan
[4]Departments of Genetics and Pathology, Stanford University, Stanford, CA 94305, USA
[5]These authors contributed equally
[6]Lead contact
*Correspondence: shimon@ifrec.osaka-u.ac.jp
https://doi.org/10.1016/j.immuni.2021.04.005

SUMMARY

The transcription factor Foxp3 plays crucial roles for Treg cell development and function. Conserved non-coding sequences (CNSs) at the *Foxp3* locus control *Foxp3* transcription, but how they developmentally contribute to Treg cell lineage specification remains obscure. Here, we show that among *Foxp3* CNSs, the promoter-upstream CNS0 and the intergenic CNS3, which bind distinct transcription factors, were activated at early stages of thymocyte differentiation prior to *Foxp3* promoter activation, with sequential genomic looping bridging these regions and the promoter. While deletion of either CNS0 or CNS3 partially compromised thymic Treg cell generation, deletion of both completely abrogated the generation and impaired the stability of Foxp3 expression in residual Treg cells. As a result, CNS0 and CNS3 double-deleted mice succumbed to lethal systemic autoimmunity and inflammation. Thus, hierarchical and coordinated activation of *Foxp3* CNS0 and CNS3 initiates and stabilizes *Foxp3* gene expression, thereby crucially controlling Treg cell development, maintenance, and consequently immunological self-tolerance.

INTRODUCTION

Naturally occurring $CD25^+CD4^+$ regulatory T (Treg) cells, which are indispensable for the establishment and maintenance of immunological self-tolerance and homeostasis, specifically express the transcription factor (TF) Foxp3 (Josefowicz et al., 2012a; Sakaguchi et al., 2008). Although the majority of $Foxp3^+$ Treg cells are produced by the thymus (thymus-derived Treg [tTreg] cells), some are physiologically induced in the periphery (peripherally derived Treg [pTreg] cells) from conventional T (Tconv) cells. Mutations of the *Foxp3* gene cause severe autoimmune diseases (e.g., type 1 diabetes), allergy, and immunopathology (e.g., inflammatory bowel disease) in humans and rodents, illustrating the crucial function of Foxp3 in Treg cell-mediated maintenance of immunological self-tolerance and homeostasis (Godfrey et al., 1991; Wildin et al., 2001). Foxp3 is a master regulator of Treg cell-specific functions, and its ectopic expression is able to confer suppressive activity on Tconv cells (Hori et al., 2003; Fontenot et al., 2003). Upon activation of natural Treg cells, Foxp3 acts as a strong repressor and downregulates genes such as *Il2* and *Ifng* but can also act as an activator in upregulating other genes, such as *Il2ra* and *Ctla4* (Morikawa et al., 2014; Ohkura et al., 2012; Samstein et al., 2012). This functional duality of Foxp3 allows a tightly regulated transcriptional program that enables fine-tuned control over Treg cell function and identity. In addition to Foxp3 expression, Treg cells possess Treg cell-specific epigenetic signatures such as DNA hypomethylation and histone modification at Treg cell function-associated gene loci, including the *Foxp3* locus. The formation of the Treg cell-specific epigenetic pattern starts in early stages of thymic Treg cell generation before the expression of *Foxp3* and other Treg cell signature genes (Kitagawa et al., 2017; Ohkura and Sakaguchi, 2020) and has been shown to be independent of Foxp3 expression, as illustrated by its presence in Foxp3-deficient mice (Ohkura et al., 2012). However, how Treg cell signature gene loci, in particular the *Foxp3* locus, become activated along Treg cell differentiation in the thymus remains to be addressed.

At the *Foxp3* gene locus, the mammalian conserved non-coding sequences (CNSs) have been highlighted as the key functional enhancer elements for induction and stabilization of Foxp3 expression (Kim and Leonard, 2007; Tone et al., 2008; Zheng et al., 2010). Among the three intergenic CNSs in *Foxp3* intron 1, CNS1 contains the transforming growth factor-β (TGF-β) response element, which contributes to extrathymic Treg cell generation and mucosal immune tolerance (Josefowicz et al., 2012b); CNS2 is responsible for the stability of Foxp3 in response to T cell receptor (TCR)

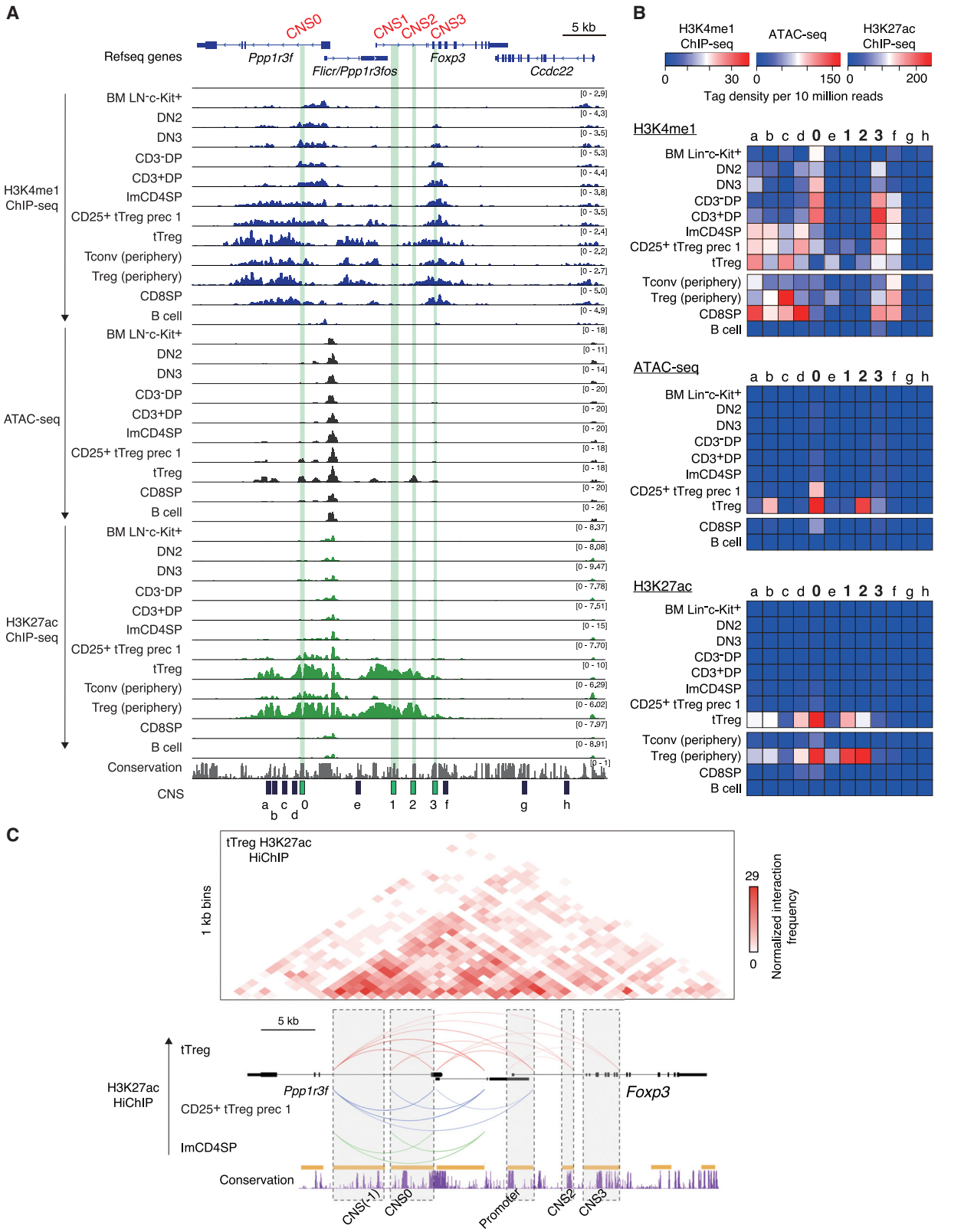

(legend on next page)

stimulation (Feng et al., 2014; Li et al., 2014); and CNS3 apparently plays a role in thresholding TCR stimuli required for Foxp3 expression (Feng et al., 2015). In addition, CNS0 upstream of *Foxp3* transcription start site (TSS) has recently been identified (Kitagawa et al., 2017). This region has been reported to be bound by various chromatin modifiers and TFs, such as the genome organizer Satb1, the histone methyl transferase MLL-4, the non-canonical BAF chromatin-modifying complex component Brd9, and signal transducer and activator of transcription (STAT) 5 (Akamatsu et al., 2019; Kitagawa et al., 2017; Loo et al., 2020; Placek et al., 2017). Although these CNSs have been linked with enhancer functions for *Foxp3* gene expression, each single CNS has thus far appeared to be mostly dispensable for thymic Treg cell generation because CNS0-, CNS1-, CNS2-, or CNS3-deficient mice grow normally, with only a slight reduction in Foxp3$^+$ Treg cells (Feng et al., 2014, 2015; Josefowicz et al., 2012b; Placek et al., 2017; Zheng et al., 2010). On the other hand, we have previously shown that Treg cell-specific super-enhancers, as dense clusters of multiple enhancers, are gradually and concurrently activated from the precursor stage before Foxp3 expression at several Treg cell signature genes such as *Foxp3*, *Il2ra*, and *Ctla4*, during the course of tTreg cell development (Kitagawa et al., 2017). Disruption of super-enhancer activation in these gene loci by deleting *Satb1* from the CD4/CD8 double-positive (DP) stage onward severely impairs tTreg cell development, resulting in the occurrence of severe autoimmune diseases. These findings, when taken together, suggest that dynamic and cooperative interactions among multiple enhancers in the *Foxp3* CNS regions are critically important for proper *Foxp3* gene expression and consequent Treg cell generation, function, and maintenance.

In this report, we address how the *Foxp3* CNS elements become sequentially activated in developing tTreg cells at various stages before and after receiving TCR signal for their differentiation; how Foxp3 expression is specifically controlled by dynamic epigenetic alterations, chromatin configuration changes, and TF binding at the enhancers, as well as spatial interactions among the enhancers via genomic looping; and whether the deletion of CNSs, individually or in combination, affects Treg cell development and maintenance, thereby breaching immunological self-tolerance and homeostasis.

RESULTS

Foxp3 CNS0 and CNS3 become activated with enhancer looping in early stages of Treg cell development

To identify regulatory regions associated with *Foxp3* gene expression along tTreg cell development, we first examined the primed enhancer histone mark H3K4me1, the activated enhancer histone mark H3K27ac, and chromatin accessibility in lymphocytes at different developmental stages: Lin$^-$c-Kit$^+$ bone marrow (BM) progenitors, c-Kit$^+$CD25$^+$ CD4/CD8 double-negative (DN) (i.e., DN2) thymocytes, c-Kit$^-$CD25$^+$DN (i.e., DN3) thymocytes, CD3$^-$ early DP thymocytes, CD3$^+$ late DP thymocytes, CD8 single-positive (CD8SP) thymocytes, CD24^{hi} immature CD4SP (imCD4SP) thymocytes, CD25$^+$Foxp3$^-$ tTreg precursor cells (Prec), CD25$^+$Foxp3$^+$ tTreg cells, and splenic CD19$^+$MHCII$^+$ B cells (Figures 1A and 1B; Figure S1A). At the *Foxp3* locus, we found that CNS0 and CNS3 were marked by H3K4me1 from the DN2 stage (DN1 thymocytes were too small in number to analyze using chromatin immunoprecipitation sequencing [ChIP-seq]). In contrast, H3K27ac histone modification and chromatin accessibility were low, indicating that these regions were primed, but not yet fully activated at these stages. The mark was also detected in CD8SP thymocytes, but not in CD19$^+$ B cells, suggesting that this epigenetic feature was unique for T-lineage cells. DP thymocytes at an early (CD3$^-$TCR-β^-) or a late (CD3$^+$TCR-β^+) stage were similar in H3K4me1 modification pattern, indicating that this enhancer priming was independent of TCR signaling. In line with this observation, DN2 thymocytes collected from *Rag2*-deficient mice, in which DN thymocytes do not receive TCR signal, similarly exhibited the H3K4me1 primed enhancer mark at the *Foxp3* CNS0 and CNS3 (Figure S1B) and at enhancer regions of other Treg cell signature genes (data not shown).

We next assessed the developmental kinetics of functional enhancer-promoter and enhancer-enhancer *cis*-looping using H3K27ac HiChIP (Mumbach et al., 2016) in immature CD4SP cells, CD25$^+$Foxp3$^-$ tTreg precursor cells, and CD25$^+$Foxp3$^+$ tTreg cells in the thymus (Figure 1C). The analysis revealed that H3K27ac-centric enhancer looping of CNS0 and an adjacent CNS cluster, designated CNS(−1) (annotated by dotted lines in Figure 1C), with a near proximal region of the *Foxp3* TSS-promoter began in immature CD4SP thymocytes. From the tTreg precursor cells to the Foxp3$^+$ tTreg cell stage, additional *de novo cis*-interactions gradually occurred among CNS0, CNS(−1), the CNS elements located in *Foxp3* gene body (such as CNS2 and CNS3), and the TSS-promoter.

Taken together, these results indicate that the CNSs within the *Foxp3* super-enhancer acquire epigenetically primed enhancer statuses in the course of Treg cell development in the thymus, starting at the DN stage in a TCR stimulation-independent manner. *Cis*-interaction of CNS0 or CNS(−1) with the regions proximal to the *Foxp3* promoter started at immature CD4SP stage or before, followed by an increase of *de novo* enhancer-enhancer and enhancer-promoter interactions involving CNS3 at the tTreg cell stage, culminating in the activation of the Foxp3 enhancer cluster.

Figure 1. *Foxp3* CNS0 and CNS3 become activated with enhancer looping in early stages of Treg cell development

(A) H3K4me1 ChIP-seq, H3K27ac ChIP-seq, and ATAC-seq peak call near murine *Foxp3* gene locus in the course of T cell development. Mammalian conservation score is provided from UCSC mm9. Data show a representative result of at least two independent experiments or from previous publication (Kitagawa et al., 2017).

(B) Quantified H3K4me1 ChIP-seq, H3K27ac ChIP-seq, and ATAC-seq tag density at indicated Foxp3-CNS regions. Heatmap shows ChIP-seq or ATAC-seq read counts normalized to 10 million mapped reads. Data show a representative result of at least two independent experiments or from previous publication (Kitagawa et al., 2017).

(C) H3K27ac HiChIP within *Foxp3* locus in thymic immature CD4SP, CD25$^+$ tTreg cell precursor 1, and CD25$^+$Foxp3$^+$ tTreg cells. Normalized interaction frequency within 1 kb bins is shown as heatmap. The certainty of looping between each anchor within the *Foxp3* locus is indicated by the density of lines. Data show a representative result of two independent experiments. Scale bar, 5 kb.

Also see Figure S1 and Data S1, S2, S3, and S4.

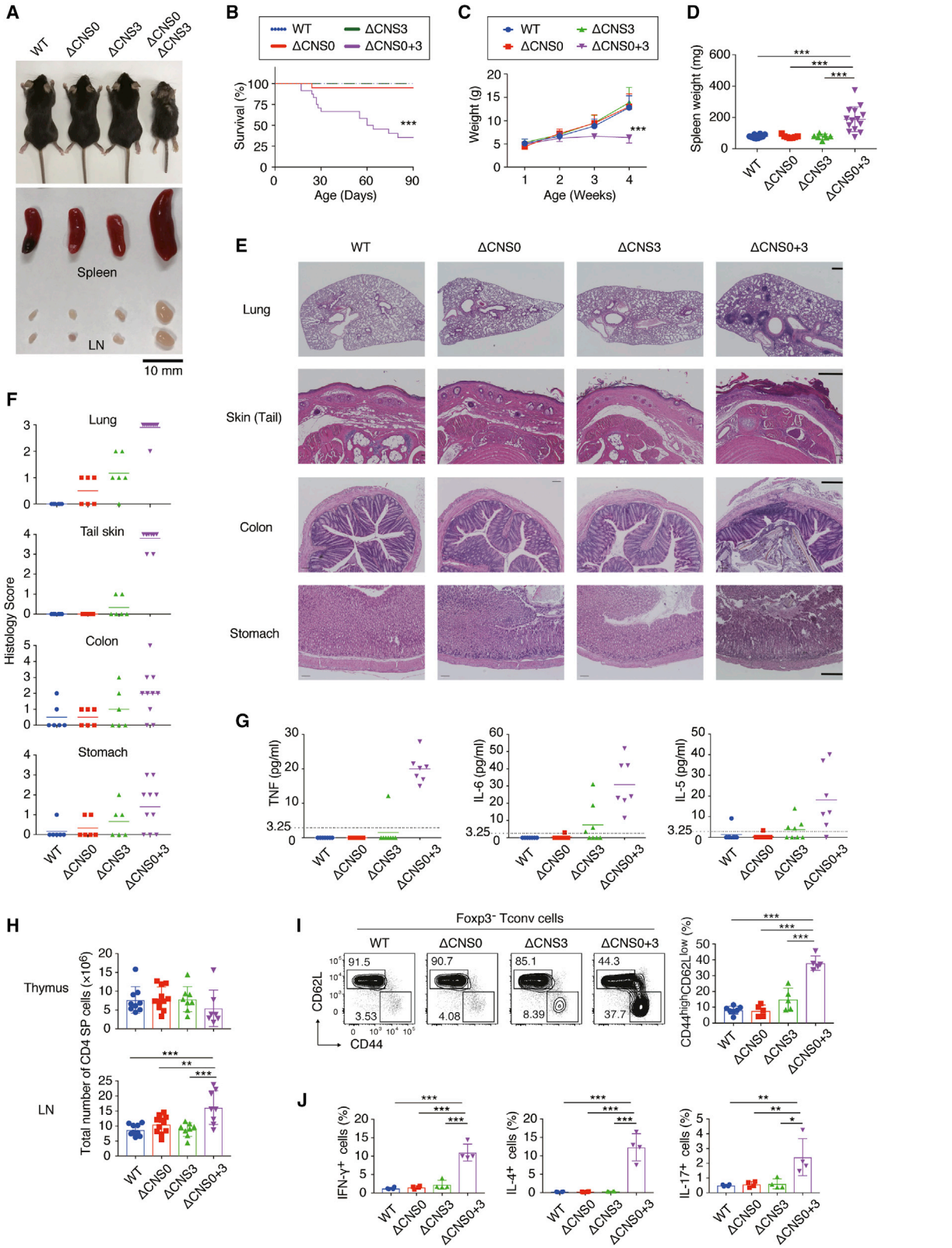

Figure 2. Deletion of both CNS0 and CNS3 causes severe autoimmunity

Phenotypes of wild-type (WT), CNS0, CNS3, or CNS0+3 double-deficient mice on the C57BL/6 Foxp3-IRES-DTR-GFP (FDG) background.

(A) A representative appearance of whole body, spleen, and inguinal lymph nodes (LNs) at 4 weeks of age. Data from at least 20 mice of each. Scale bar, 10 mm.

(legend continued on next page)

Deletion of both CNS0 and CNS3 causes severe autoimmunity

To investigate the respective roles of CNS0 and CNS3 *in vivo*, we next generated the mouse strains with specific deletion of CNS0 or CNS3, or both, using CRISPR-Cas9 genome editing (Figure S2A). In concordance with previous reports, CNS0 or CNS3 single-deficient (ΔCNS0 or ΔCNS3) mice grew normally without apparent inflammation (Feng et al., 2015; Placek et al., 2017), even at old age (~12 months; data not shown). In contrast, CNS0 and CNS3 double-deficient (ΔCNS0+3) mice exhibited poor survival, reduced weight and body size, splenomegaly, and lymph adenopathy (Figures 2A–2D). ΔCNS0+3 mice developed spontaneous lethal systemic autoimmune inflammation with histologically evident inflammation in the lung, skin, colon, and stomach (Figure 2E) with high histological scores (Figure 2F). Serum concentrations of interleukin-5 (IL-5), IL-6, and tumor necrosis factor (TNF) were high in ΔCNS0+3 mice (Figure 2G). Moreover, serum autoantibodies specific for gastric parietal cells or double-stranded DNA as typical examples of organ-specific and systemic autoimmunity, respectively, developed in ΔCNS0+3 mice and to a lesser extent in ΔCNS3 mice (Figure S2B).

The total numbers and percentages of $CD4^+$ T and $CD8^+$ T cells in the thymus were not different among ΔCNS0, ΔCNS3, and ΔCNS0+3 mice (Figure 2H and data not shown). The number of peripheral $CD4^+$ T cells, in particular $CD44^+$ $CD62L^-$ activated or memory $CD4^+$ T cells, was significantly increased in ΔCNS0+3 mice, likely reflecting their involvement in inflammation (Figures 2H and 2I). Consistently, $CD4^+$ Tconv cells in ΔCNS0+3 mice produced inflammatory cytokines such as interferon-γ (IFN-γ), IL-4, and IL-17 (Figure 2J).

Collectively, simultaneous deletion of both CNS0 and CNS3 induces autoimmune and inflammatory diseases similar to those produced by Treg cell depletion in normal mice (e.g., colitis and autoimmune gastritis) (Sakaguchi et al., 1995).

Deletion of CNS0 or CNS3, especially both, impairs tTreg, pTreg, and iTreg cell generation

Flow cytometric analysis of thymocytes and peripheral lymphocytes in ΔCNS0, ΔCNS3, and ΔCNS0+3 mice revealed a severe reduction of Treg cells in ΔCNS0+3 mice in both number and percentage among CD4SP thymocytes and peripheral $CD4^+$ T cells, with an increase in peripheral $CD25^+CD4^+$ Tconv cells presumably involved in the autoimmune inflammation (see above) (Figure 3A). ΔCNS0 or ΔCNS3 mice also showed a reduction of Treg cells in the thymus by ~50% and in the periphery by ~30%. In addition, the thymic $CD25^+Foxp3^-$ tTreg cell precursor 1 population was significantly increased in ΔCNS0+3 mice, with significant reduction of the $CD25^-Foxp3^+$ precursor 2 population (Figure 3B).

These results prompted us to investigate the potential of $CD25^+Foxp3^-$ thymic Treg precursor cells in ΔCNS0, ΔCNS3, or ΔCNS0+3 mice to differentiate into $Foxp3^+$ cells in the presence of TCR stimulation and IL-2 (Figure 3C), IL-2 alone (Figure S3A), or IL-2 and IL-7, with or without TNF-α *in vitro* (Figure S3B). We found a marked defect in the ability of Treg precursor cells to give rise to $Foxp3^+$ cells in all three mouse strains under these conditions. Similarly, *in vivo* induction of pTreg cells by transferring $Foxp3^-CD62L^{hi}CD44^{lo}$ naive $CD4^+$ Tconv cells from ΔCNS0, ΔCNS3, or ΔCNS0+3 mice into *Rag2*$^{-/-}$ mice resulted in a failure to generate pTreg cells. Moreover, CNS-deficient, especially ΔCNS0+3, mice were severely impaired in *in vitro* generation of induced Treg (iTreg) cells from naive Tconv cells in the presence of TGF-β, IL-2, and TCR stimulation, which could not be rescued by varying IL-2 dose or TCR or co-stimulation strength (Figures S3C and 3D).

To further assess the developmental arrest of Treg cells *in vivo* in CNS-deleted T cells, we generated mixed BM chimera with $CD45.1^+$ wild-type (WT) BM cells and congenic $CD45.2^+$ ΔCNS0, ΔCNS3, or ΔCNS0+3 BM cells (Figures 3D and 3E). Compared with the WT counterparts, ΔCNS0, ΔCNS3, and in particular ΔCNS0+3 thymocytes and splenic T cells were severely deficient in Treg cells (Figure 3E), with an increase of thymic $Foxp3^-CD25^+GITR^+$ tTreg precursor 1 cells and a reduction of $Foxp3^+CD25^-$ precursor 2 cells (Figure 3F).

Collectively, these data clearly indicate that CNS0 and CNS3, especially in combination, are required for tTreg cell differentiation from the precursor 1 population and for the generation of the precursor 2 population in the thymus, and also for pTreg and iTreg cell development from Tconv cells *in vivo* and *in vitro*, respectively.

CNS regions provide the platforms for binding of nuclear proteins to form the Foxp3 enhancer cluster

We next sought to examine whether CNS0 or CNS3 deficiency could affect H3K4me1-marked primed enhancer formation at the CNS3 or CNS0 region, respectively. In these ΔCNS mice, H3K4me1 modification and ATAC-seq signal were abrogated only in the deleted regions because the corresponding DNA sequences were absent (Figure 4A). CNS0 or CNS3 deletion did not influence the primed enhancer status CNS3 or CNS0, respectively, at least at the thymic DP and immature CD4SP stages, suggesting that H3K4me1 priming at each CNS region was independently controlled. In addition, although H3K4me1 mark was not clearly segregated between the CNS0 region and the *Ppp1r3f*

(B) Kaplan-Meier survival curve from birth to 90-day-old mice (n = 14–20).
(C) Body weight of 1- to 4-week-old mice (n = 7–12).
(D) Spleen weight at 4- to 6-week-old mice (n = 10).
(E and F) Tissue histology of lung, stomach, colon, and tail skin of 8- to 12-week-old mice (H&E staining). A representative image (E) and scoring of tissue pathology described as means with individual values (F) of 6 each of WT, ΔCNS0, or ΔCNS3 mice and 10 ΔCNS0+3 mice. Scale bar, 200 μm.
(G) Serum concentrations of inflammatory cytokines (TNF, IL-6, IL-5) determined by BD cytometric bead array assay. The detection limit of 3.25 pg/mL is depicted in the graph as a dotted line. Data show means with individual values (n = 7 or 8).
(H) Total cell numbers of $CD4^+CD8^-$ T cells in CNS-deficient mice in the thymus and periphery.
(I) Effector/naive proportions among peripheral $CD4^+Foxp3^-$ conventional T cells determined using flow cytometry at 8 weeks of age.
(J) Percentages of IFN-γ-, IL-4-, and IL-17-producing cells among whole $CD4^+$ cells in peripheral LNs determined using flow cytometry at 8 weeks of age.
Bar graphs show means with SDs. *$p < 0.05$, **$p < 0.01$, and ***$p < 0.001$ (log-rank test in B, two-way ANOVA followed by Tukey's multiple-comparison test in C, and one-way ANOVA followed by Tukey's multiple-comparison test in D and H–J). Also see Figure S2.

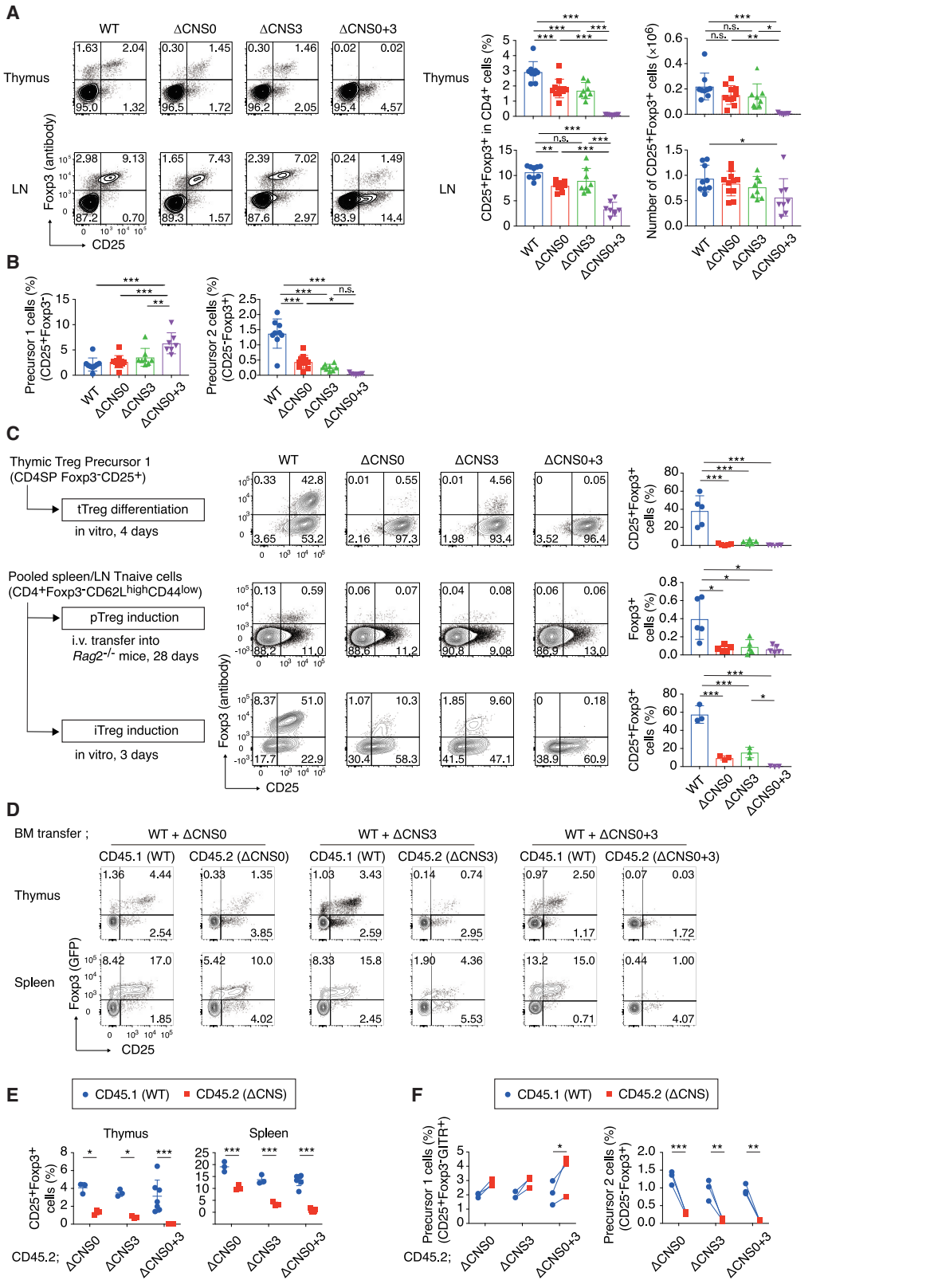

(legend on next page)

gene promoter, chromatin accessibility data clearly separated these regions, suggesting that CNS0 is an independent enhancer unit, discontinuous from the *Ppp1r3f* gene promoter.

During tTreg cell development from CD4SP thymocytes, via the $CD25^+Foxp3^-$ precursor 1 and $CD25^-Foxp3^+$ precursor 2 populations, chromatin accessibility was increased at CNS0, CNS2, and CNS3 (Figure 4B). To examine possible contribution of TCR and IL-2 stimulation in the activation of *Foxp3* CNS elements, we stimulated $CD24^{hi}$ immature CD4SP thymocytes *in vitro* with anti-CD3 and anti-CD28 beads and IL-2, TCR stimulation alone (i.e., anti-CD3 and anti-CD28 beads and anti-IL-2), or IL-2 alone (Figure 4B). The combination of IL-2 and TCR stimulation enhanced chromatin accessibility of CNS0 and CNS(−1) compared with TCR treatment or IL-2 treatment alone, while chromatin accessibility of CNS2 and CNS3 located within the Foxp3 gene body was not evident. These results collectively indicate that a combination of TCR and IL-2 stimuli can partially recapitulate the activation of Foxp3 enhancer elements along tTreg cell differentiation.

To further address the possible division of labor between CNS0 and CNS3 in the induction and maintenance of Foxp3 expression, we conducted an *in silico* search for TFs possessing compatible DNA binding motifs within the CNSs at the *Foxp3* locus. Consensus TF binding motif scanning using the JASPAR database predicted potential binding proteins, which included TFs previously reported to be essential for Treg cell generation and the maintenance (e.g., STAT, Runx1, ETS, NFKB; Figure S4A). Furthermore, we experimentally confirmed the binding of STAT5, ETS1, Rela/p65, Creb, Runx1, and Foxp3 to CNSs in Treg cells and not in Tconv cells using ChIP-seq (Figure S4B). Many factors showed similar binding distributions, with major peaks at CNS0 and CNS2, in concordance with previous studies showing binding of Stat5, Runx1, and Foxp3 to these CNSs (Akamatsu et al., 2019; Kitagawa et al., 2017; Placek et al., 2017). In contrast, nuclear protein binding to CNS3 was not evident except for ETS1 and Rela/p65, which showed weak binding.

Taken together, these results suggest that CNS0 and CNS3, which provide platforms for binding distinct nuclear proteins, are independently and distinctly regulated despite the synchronized timing of their activation and similar impacts on Treg cell development when deleted.

CNS0 and CNS3 contribute to tTreg cell differentiation

We next addressed how CNS0 and CNS3 enhancer regions were involved in induction of Foxp3 expression by TCR and IL-2 stimulation, two signals crucial for tTreg cell development, at immature CD4SP stage. We generated CNS0- or CNS3-deficient mice expressing a Foxp3-hCD2 reporter and crossed them with DEREG BAC-transgenic mice expressing diphtheria toxin receptor-fused GFP under the Foxp3 promoter (Lahl et al., 2007; Figure 5A). We reasoned that because the DEREG BAC-GFP transgene construct contained WT *Foxp3* promoter and enhancer elements including CNS0, CNS1, CNS2, and CNS3, resulting GFP expression could be used as a surrogate readout for cell-intrinsic signaling of Foxp3 expression (Ohkura et al., 2012). In contrast with WT mice, in which the majority of GFP^+ cells were also $hCD2^+$ in the CD4SP thymocyte population and peripheral $CD4^+$ T cells, a substantial number of GFP^+hCD2^- cells emerged in the thymus and the periphery of ΔCNS0 or ΔCNS3 mice, especially in the latter (Figure 5B). The expression of Treg cell function-associated molecules (e.g., CTLA-4, GITR, OX-40, FR4, Nrp-1, Helios) were much lower in the GFP^+hCD2^- population compared with the GFP^+hCD2^+ population in the thymus of CNS-deficient mice (Figure 5C). These results indicate that either CNS0 or CNS3 deficiency profoundly impairs the ability of developing Treg cells to upregulate Foxp3 expression despite receiving appropriate signaling for Foxp3 transcription.

We then assessed the ability of GFP^-hCD2^-, GFP^+hCD2^-, and GFP^+hCD2^+ CD4SP thymocytes in CNS-deficient mice, as shown in Figure 5B, to differentiate into $Foxp3^+$ T cells upon *in vitro* TCR and IL-2 stimulation or IL-2 stimulation alone. Anti-CD3, anti-CD28, and IL-2 stimulation of WT GFP^-hCD2^- thymocytes induced ~20% GFP^+hCD2^+ cells, whereas IL-2 stimulation alone induced only a few (~5%) (Figure 5D). Similar stimulation of ΔCNS0 or ΔCNS3 GFP^-hCD2^- thymocytes comparably induced GFP^+hCD2^- cells, but not GFP^+hCD2^+ cells (Figure 5D). Stimulation of GFP^+hCD2^- thymocytes in ΔCNS3 mice generated GFP^+hCD2^+ cells either by anti-CD3, anti-CD28 and IL-2, or IL-2 alone; in contrast, either way of stimulation of ΔCNS0 GFP^+hCD2^+ cells failed in the generation (Figure 5E). This indicated that ΔCNS0 GFP^+hCD2^- thymocytes were unresponsive to IL-2 stimulation, while ΔCNS3 GFP^+hCD2^- cells were IL-2 responsive and could differentiate into $hCD2^+$ cells without requiring TCR stimulation. Notably, ΔCNS3 GFP^+hCD2^- cells contained a higher percentage of $CD25^+$ cells compared with the ΔCNS0 counterpart (Figure S5A), but separation of ΔCNS0 or ΔCNS3 GFP^+hCD2^- cells into $CD25^+$ and $CD25^-$ populations did not alter the trend that ΔCNS3, but not ΔCNS0 GFP^+hCD2^- cells were able to produce $hCD2^+$ cells upon stimulation

Figure 3. Deletion of CNS0 or CNS3, especially both, impairs tTreg, pTreg, and iTreg cell generation

(A) Percentages and total cell numbers of $CD25^+Foxp3^+$ Treg cells in the thymus and in pooled peripheral lymph nodes of 4-week-old mice (n = 7–10).

(B) Percentages of thymic Treg cell precursor fractions in CD4SP thymocytes of 4-week-old mice; $CD25^+Foxp3^-$ (precursor 1) and $CD25^-Foxp3^+$ (precursor 2) (n = 7–10).

(C) Top row: *in vitro* induction of thymic Treg cells. Sorted $CD25^+Foxp3\text{-}GFP^-$ CD4SP cells (tTreg precursor cell 1) were stimulated with anti-CD3 and anti-CD28 beads and 100 U/mL of IL-2 for 4 days (n = 5). Middle row: *in vivo* induction of pTreg cells. $CD4^+$ naive T cells were intravenously (i.v.) transferred into *Rag2*-deficient recipients. Mesenteric lymph nodes were collected and analyzed using flow cytometry 4 weeks after transfer (n = 5). Bottom row: *in vitro* induction of iTreg cells from naive $CD4^+$ T cells by stimulation with plate-bound anti-CD3, anti-CD28, 50 U/mL IL-2, and 2.5 ng/mL TGF-β for 3 days (n = 3).

(D and E) Mixed bone marrow chimeric mice of $CD45.1^+$ WT and $CD45.2^+$ CNS-deficient BM cells. Thymuses and spleens were harvested and analyzed 5 weeks after transfer (n = 3–7).

(F) Frequencies of thymic Treg precursor 1 ($CD25^+Foxp3^-GITR^+$cells) and precursor 2 ($CD25^-Foxp3^+$) among CD4SPs in indicated BM transfers (n = 3).

Percentages of cell populations were determined using flow cytometry. Bar graphs show means with SDs. *$p < 0.05$, **$p < 0.01$, ***$p < 0.001$, and n.s., not significant (one-way ANOVA followed by Tukey's multiple-comparison test in A–C, two-way ANOVA followed by Sidak's multiple-comparison test in D–F). Also see Figure S3.

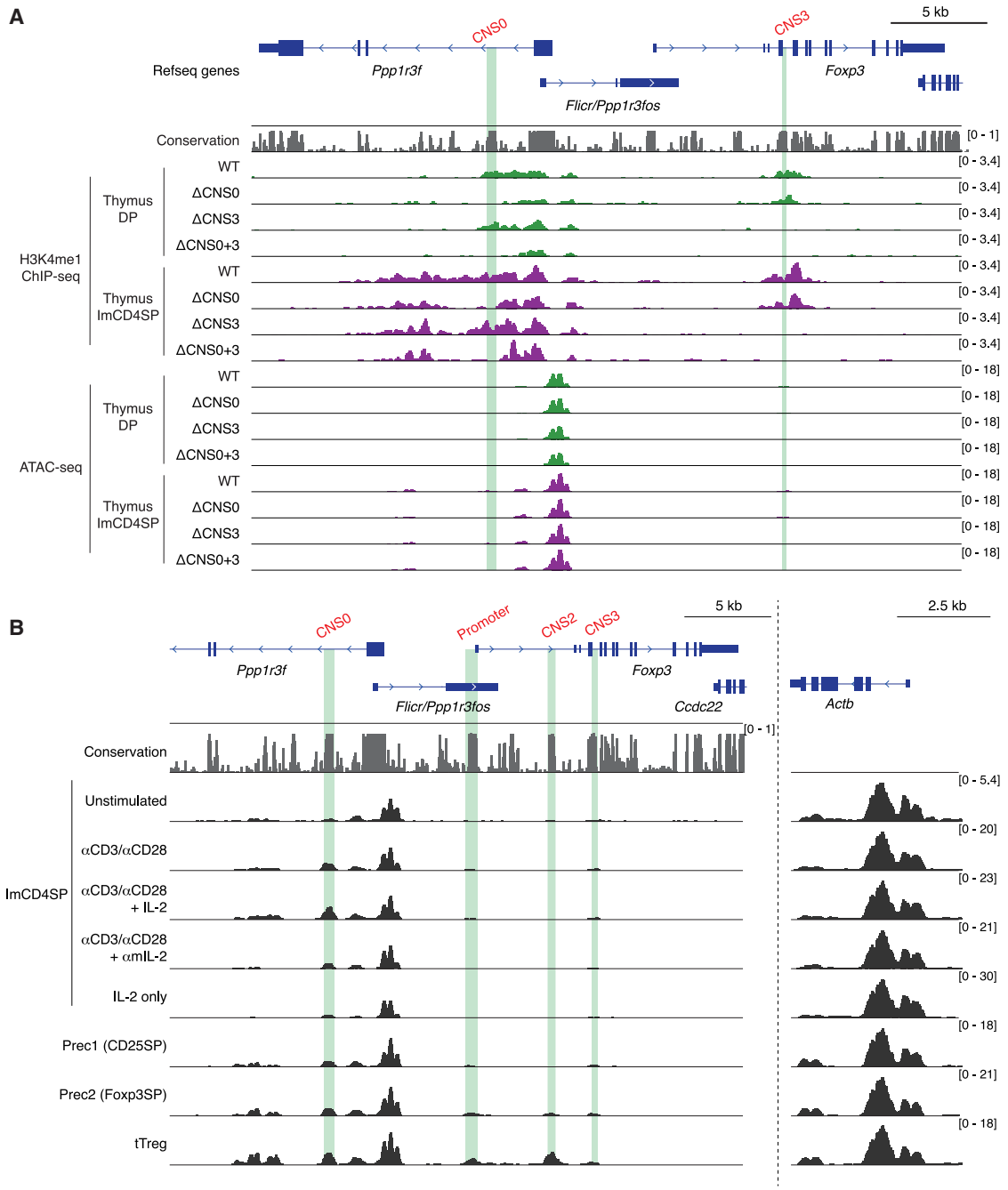

Figure 4. CNS regions provide the platforms for binding of nuclear proteins to form Foxp3 enhancer cluster

(A) H3K4me1 ChIP-seq and ATAC-seq performed with thymic DP and immature CD4SP cells from WT or CNS-deficient mice. Data are from independently performed two experiments for each cell population or from previous publication (WT DP and WT immature CD4SP cells; Kitagawa et al., 2017).

(B) ATAC-seq performed with thymic immature CD4SP cells (*ex vivo* or stimulated *in vitro* for 18 h), $CD25^{+}Foxp3^{-}$ tTreg precursor 1 cells, $CD25^{-}Foxp3^{+}$ tTreg precursor 2 cells, and $CD25^{+}Foxp3^{+}$ tTreg cells. Immature CD4SP cells were cultured in indicated conditions; the presence or absence of anti-CD3 and anti-CD28 beads, 100 U/mL IL-2, or 2.5 μg/mL of anti-IL-2 neutralizing antibody. Called peaks were normalized to *Actb* locus in IGV genome browser. Data are representative results from two to four independent experiments.

Also see Figure S4 and Data S1, S2, and S3.

(Figure S5B). These results collectively indicate that TCR stimulation is required for the initial activation of CNS0 and CNS3 and that CNS0 is indispensable for IL-2 responsiveness in tTreg cell differentiation, while CNS3 is not, consistent with the finding that CNS0, but not CNS3, was a major binding site of Stat5 at the *Foxp3* locus (Figure S4B).

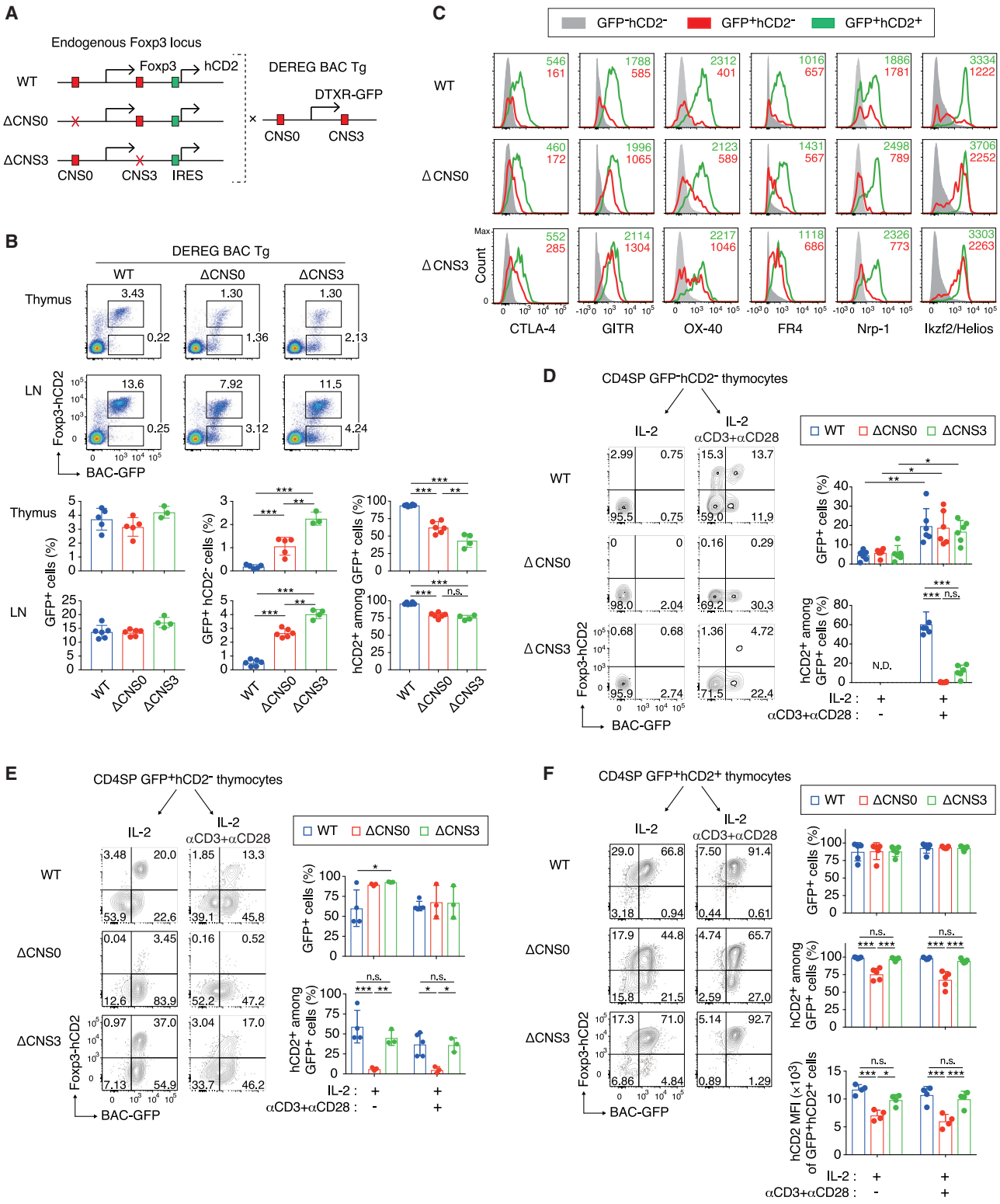

Figure 5. Contribution of CNS0 and CNS3 to tTreg cell differentiation

(A) Schematic diagram of the experimental system to detect cells receiving signals for Foxp3$^+$ tTreg cell development. ΔCNS0 or ΔCNS3 mice on the C57BL/6 Foxp3-hCD2 reporter background were crossed with DEREG-BAC Tg mice.

(legend continued on next page)

We next examined the roles of CNS0 and CNS3 in the maintenance of Foxp3 expression in mature tTreg cells. In the presence of IL-2, WT GFP$^+$hCD2$^+$ cells stably expressed GFP and hCD2 (i.e., Foxp3$^+$) at least for 6 days *in vitro*. Although ΔCNS3 GFP$^+$ hCD2$^+$ cells were similarly stable in this setting, ΔCNS0 GFP$^+$ hCD2$^+$ cells comparably retained GFP expression but showed a reduction in the expression of hCD2 and the percentage of hCD2$^+$ cells; that is, ~30% of GFP$^+$hCD2$^+$ cells lost hCD2 expression even in the presence of continuous IL-2 and TCR stimulation (Figure 5F). This suggested that GFP$^+$hCD2$^-$ cells found in CNS-deficient mice (Figure 5B) might contain ex-Treg cells derived from GFP$^+$hCD2$^+$ Treg cells. In addition, as the functional stability in WT mature tTreg cells has been shown to be linked with the presence of Treg cell-specific CpG demethylation at the *Foxp3* CNS2 region (Floess et al., 2007; Ohkura et al., 2012; Polansky et al., 2008), we assessed CNS2 methylation status of CD25$^+$hCD2$^+$ tTreg cells in CNS-deficient mice and found that CNS2 demethylation status was comparable among WT, ΔCNS0, and ΔCNS3 mice (Figure S5C). The results indicate that CNS0, but not CNS3, is required for the stability of tTreg cells, in a CNS2 demethylation-independent manner.

CNS0 and CNS3 contribute to peripheral Treg cell stability

The above results indicating the instability of Foxp3 expression in thymic CNS-deficient tTreg cells prompted us to address *in vivo* and *in vitro* stability of Foxp3 expression and function of peripheral Treg cells in CNS-deficient mice.

Flow cytometric analysis revealed that CNS-deficient especially ΔCNS0+3 peripheral Treg cells were higher than the WT counterpart in the expression of CD44, CTLA-4, TIGIT, OX-40, ICOS, KLRG1, and Ki-67 (Figure S6A). Thus CNS-deficient Treg cells were not hampered in the expression of essential Treg cell signature genes, except for Foxp3, and exhibited more activated phenotypes. The phenotype could be attributed in part to a secondary effect of the autoimmune and inflammatory condition of CNS-deficient mice and to a possibly more self-reactive TCR repertoire of CNS-deficient Treg cells, as previously suggested with CNS3-deficient mice (Feng et al., 2015).

To assess *in vitro* stability of Foxp3 expression in CNS-deficient Treg cells, we stimulated purified Foxp3$^+$CD25$^+$CD4$^+$ splenic Treg cells for 3 or 6 days by anti-CD3 and IL-2 and found that ΔCNS0+3 Treg cells and, to a lesser extent, ΔCNS0 Treg cells gradually lost Foxp3 expression (Figure 6A). This effect was not observed in ΔCNS3 Treg cells, and the reduction of Foxp3 was dependent on proliferation (data not shown), similar to CNS2-deficient mice (Feng et al., 2014). Although CNS2 hypomethylation was not reduced in ΔCNS0 Treg cells 6 days poststimulation, it was marginally reduced in ΔCNS0+3 Foxp3$^+$ Treg cells and markedly in the ΔCNS0+3 Foxp3$^-$ (ex-Foxp3$^+$) fraction (Figure 6B).

Next, to assess *in vivo* stability of CNS-deficient Treg cells, we co-transferred CD45.2$^+$ ΔCNS Treg cells and CD45.1$^+$ CD4$^+$ CD45RB^{hi} naive Tconv cells in a 1:1 ratio into *Rag2*$^{-/-}$ mice. After 56 days, transferred CD45.2$^+$ WT, ΔCNS0, or ΔCNS3 Treg cells retained Foxp3 expression; however, Foxp3-expressing ΔCNS0+3 Treg cells were reduced in percentage (Figures 6C and 6D) and also in their intensity of Foxp3 expression (Figure 6E). In these cell transfer experiments, the degree of CNS2 demethylation in the CD25$^+$ fraction of WT and ΔCNS0+3 Treg cells shown in Figure 6C was comparably high (Figure 6F), although the latter showed significantly reduced Foxp3 expression (Figure 6E). In contrast, the degree of CNS2 demethylation was equivalently low in the CD25$^-$ fraction of WT and ΔCNS0+3 Treg cells. Thus the higher percentage of the CD25$^-$Foxp3$^-$ fraction among the transferred ΔCNS0+3 Treg cells indicated the reduction in overall CNS2 hypomethylation by CNS0 and CNS3 double deletion. Functionally, although transfer of CD4$^+$CD45RB^{hi} naive Tconv cells alone induced colitis in *Rag2*$^{-/-}$ mice, co-transfer of CNS-deficient Treg cells in a 1:1 ratio prevented colitis development (Figures S6B–S6G). With co-transfer at a lower ratio (1:8) of Treg cells versus naive Tconv cells, WT Treg cells were still able to prevent colitis, whereas ΔCNS0+3 Treg cells were not (data not shown).

In further molecular analysis, CNS2 binding of Stat5, which has been reported to control Foxp3 stability (Feng et al., 2014), was not affected in IL-2-stimulated ΔCNS0, ΔCNS3, or ΔCNS0+3 Treg cells (Figure 6G). In contrast, the intensity of H3K27ac was broadly reduced within the Foxp3 locus by ΔCNS0 or ΔCNS3 and more substantially by ΔCNS0+3, as shown representatively (Figure 6G) and quantitatively (Figure 6H).

These *in vivo* and *in vitro* results collectively indicate that CNS0 and CNS3 in combination contribute to stable maintenance of

(B) Proportion of GFP- and hCD2-expressing cells in CNS0- or CNS3-deficient thymic or peripheral CD4SP cells (n = 3–5). A representative flow cytometry plot (upper panel) and percentages of GFP$^+$ or GFP$^+$hCD2$^-$ cells among CD4SP thymocytes, and hCD2$^+$ cells among GFP$^+$ cells are shown as bar graph with means, SDs, and individual values (lower panel).

(C) Flow cytometry analysis of Treg cell signature molecules (CTLA-4, GITR, OX-40, FR4, Nrp-1, and Ikzf2/Helios) in indicated fractions of WT, ΔCNS0, or ΔCNS3 CD4SP thymocytes. MFI values of GFP$^+$hCD2$^+$ tTreg (green) and GFP$^+$hCD2$^-$ (red) cells are shown at the top right corner of each box. Data show a representative result of three independent experiments.

(D) Induction of GFP and hCD2 expression from GFP$^-$hCD2$^-$ fraction. WT, ΔCNS0, or ΔCNS3 GFP$^-$hCD2$^-$CD24^{hi} immature CD4SP thymocytes were stimulated with IL-2 with or without anti-CD3 and anti-CD28 beads *in vitro* for 6 days (n = 6). A representative flow cytometry plot of live CD4$^+$ T cells (left), the percentages of total GFP$^+$ cells among CD4$^+$ T cells (upper graph), and the percentages of hCD2$^+$ cells among GFP$^+$ cells (lower graph) are shown.

(E) Induction of hCD2 expression from GFP$^+$hCD2$^-$ fraction. Sorted GFP$^+$hCD2$^-$ cells were cultured *in vitro* in the presence of IL-2 with or without anti-CD3 and anti-CD28 beads for 6 days (n = 3–5). A representative flow cytometry plot of live CD4$^+$ cells (left), the percentages of total BAC-GFP$^+$ cells among CD4$^+$ T cells (upper graph) and the percentages of hCD2$^+$ cells among GFP$^+$ cells (lower graph) are shown.

(F) Stability of tTreg cells. Sorted GFP$^+$hCD2$^+$ tTreg cells were cultured *in vitro* in the presence of IL-2 with or without anti-CD3 and anti-CD28 beads for 6 days (n = 5). A representative flow cytometry plot of live CD4$^+$ T cells (left), the percentages of GFP$^+$ cells among CD4$^+$ T cells (upper graph), the percentages of hCD2$^+$ cells among GFP$^+$ cells (middle graph), and hCD2 MFI among hCD2$^+$ cells (lower graph) are shown.

Graphs show means with SDs. *$p < 0.05$, **$p < 0.01$, ***$p < 0.001$, and n.s., not significant (one-way ANOVA followed by Tukey's multiple-comparison test in B and two-way ANOVA followed by Sidak's multiple-comparison test in D–F). N.D., no data. Also see Figure S5.

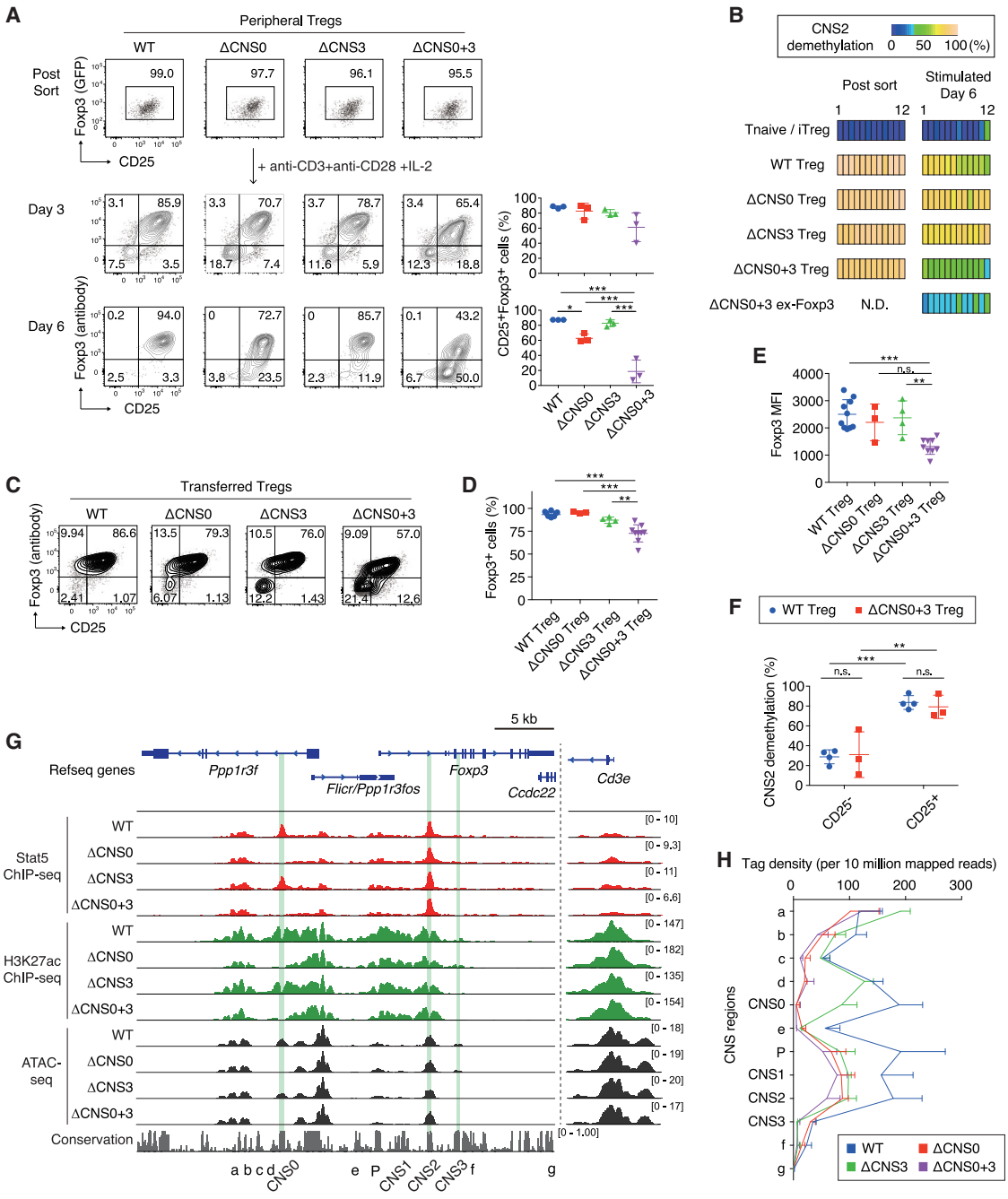

Figure 6. CNS0 and CNS3 contribute to peripheral Treg cell stability

(A) *In vitro* Foxp3 stability assay. Treg cells collected from WT, ΔCNS0, ΔCNS3, and ΔCNS0+3 mice (pooled from lymph nodes and spleen) were stimulated *in vitro* in the presence of anti-CD3 and anti-CD28 beads and IL-2 for 3 or 6 days. Percentages of $CD25^+Foxp3^+$ cells were determined using flow cytometry (n = 3).

(B) CpG DNA hypomethylation status at the *Foxp3* CNS2 locus in sorted $Foxp3^+$ cells. Treg cells from WT, ΔCNS0, ΔCNS3, and ΔCNS0+3 mice and also control naive $CD4^+$ T and iTreg cells were assessed before and after *in vitro* stimulation for 6 days. $Foxp3^-$ cells generated in the culture of ΔCNS0+3 Treg cells were also analyzed. The percentages of CpG demethylation are shown as heatmaps on 12 CpG sites. Data show a representative result of at least three independent experiments. N.D., no data.

(C–E) *In vivo* Foxp3 stability assay. $CD45.2^+CD4^+CD25^+GFP^+$ Treg cells of indicated mice were co-transferred with WT $CD45.1^+CD45RB^{hi}CD4^+$ T cells. Foxp3 expression of transferred $CD45.2^+CD4^+Foxp3^+$ cells was assessed using flow cytometry 56 days after transfer. Percentage of $Foxp3^+$ cells (D) and Foxp3 MFI (E) in $CD45.2^+$ transferred Treg cells in mesenteric LNs are shown. Foxp3 expression was analyzed using intracellular staining with anti-Foxp3 monoclonal antibody (Clone; Fjk16s) (n = 3-10).

(F) CpG DNA hypomethylation status at the *Foxp3* CNS2 locus of sorted $CD45.2^+CD4^+CD25^{+/-}$ cells from mesenteric LNs 56 days after transfer (n = 3 or 4).

(legend continued on next page)

Foxp3 expression in Treg cells and that CNS2 demethylation is installed independently of CNS0 or CNS3 enhancer activation, while the disruption of the individual Foxp3 enhancers affects the overall activity of the Foxp3 enhancer cluster and indirectly impairs the maintenance of CNS2 hypomethylation status.

DISCUSSION

Proper thymic induction of Foxp3 in Treg cell lineage commitment requires the establishment and subsequent activation of the Treg cell-specific enhancers present within the gene locus (Kitagawa et al., 2017). However, it remains poorly understood how this enhancer landscape is acquired by developing Treg cells and how the individual enhancers within the locus collectively integrate various external stimuli that ultimately lead to Foxp3 expression. In the present study, we showed that non-coding enhancer elements at the *Foxp3* locus were critical for the maintenance of immunological self-tolerance through regulation of thymic Treg cell development and function. Specifically, we demonstrated that the *Foxp3* enhancers CNS0 and CNS3 acquired characteristics of a primed epigenetic state early on in thymic T cell development and that the acquisition accompanied a gradual gain of enhancer-promoter and enhancer-enhancer H3K27ac-biased looping interactions within the *Foxp3* locus, culminating in the formation of the Foxp3 enhancer cluster. Perturbation of each enhancer function through single-enhancer deletions of CNS0 or CNS3 displayed a partial reduction in thymic Treg cell differentiation, consistent with previous studies (Placek et al., 2017; Zheng et al., 2010). In contrast, the concurrent deletion of both CNS0 and CNS3 caused profound defects in Foxp3 induction and stability, thereby severely reducing thymic and peripheral Treg cells, leading to the development of fatal autoimmune disease. In addition, we observed that CNS0 or CNS3 single deletions reduced Treg cells to one-third of WT counterparts in the thymus of BM chimera mice. These results collectively indicate that CNS0 or CNS3 single deletion substantially affects Treg cell development in the thymus but allows their compensatory expansion in the periphery to a certain extent, whereas CNS0 and CNS3 double deletion almost completely abrogates tTreg and pTreg cell development and more profoundly impairs their peripheral maintenance, presumably because of decreased stability in Foxp3 gene expression. Thus these differences between CNS0 or CNS3 single deletion and double deletion demonstrate that cooperation of CNS0 and CNS3 is critically required for immunological self-tolerance through Foxp3 induction and maintenance.

We have demonstrated the existence of an enhancer hierarchy in which the enhancers at the *Foxp3* locus are distinctly regulated at specific timings of tTreg cell development. Through H3K4me1 ChIP-seq across different developmental stages, our data indicate that the priming of enhancers at CNS0 and CNS3 are independently regulated, suggesting the possibility that they arise from different mechanisms during thymic developmental time. In contrast, our results from H3K27ac ChIP-seq in Treg cells of ΔCNS0, ΔCNS3, and ΔCNS0+3 demonstrated synergistic roles in Foxp3 enhancer activation and gene expression. Although we previously showed that Satb1 is bound and involved in enhancer activation at CNS0 and CNS3 (Kitagawa et al., 2017), additional *in silico* motif enrichment analyses of these regions and other TF ChIP-seq indicated enhancer-biased enrichment of different molecular machineries. These observations have collectively demonstrated that although the priming of individual enhancers within the Foxp3 locus occurs in an uncoupled manner, the subsequent formation and presumably maintenance of the Foxp3 enhancer cluster is facilitated by coordination among individual constituents that respond to different signaling cues. Indeed, we have demonstrated that CNS0 plays a crucial role in Treg cell development and stability through an IL-2-responsive effect dominated by Stat5, whereas CNS3 with a binding site of the NF-κB component c-Rel (Zheng et al., 2010) has been previously proposed to play a role in thresholding the strength of TCR for Treg cell development (Feng et al., 2015). Implicit in this is the existence of an enhancer hierarchy that allows the integration of specific signaling responses that critically controls Foxp3 expression. This "division of labor" hierarchy is exemplified by our observation that CNS3-deleted $GFP^{+}hCD2^{-}$ "Treg-thwarted" cells could still respond to IL-2 signaling and rescue Foxp3 expression, whereas cells harboring the deletion of the Stat5-responsive CNS0 enhancer could not. Thus, the present study has shown the importance of hierarchical and sequential activation of enhancers, which are regulated by distinct signals and factors, in a model of Treg cell differentiation.

It has been posited that thymic Treg cell differentiation from $CD25^{+}Foxp3^{-}CD4SP$ precursor cells occurs in an instructive, two-step process in which appropriate TCR signaling results in the upregulation of IL-2 proximal signaling-related molecules (Lio and Hsieh, 2008). We liken ΔCNS0+3 mice to the systematic disruption of both arms of the thymic Treg cell developmental pathway by removing the TCR stimulation-sensing CNS3 and IL-2-responsive CNS0, which can partially explain the exacerbated defect in thymic Treg cell generation observed in these mice. In addition, the markedly reduced but not completely impaired tTreg cell differentiation in ΔCNS0 and ΔCNS3 suggests that by having these two non-redundant enhancers, tTreg cell development is quantitatively and qualitatively controlled by activation of these enhancers. That is, the requirement of activating two distinct enhancers for efficient Foxp3 expression limits the range of cells that can become tTreg cells; the full spectrum of the tTreg cell functional repertoire is generated only when signals activating both CNS0 and CNS3 are present. It is therefore likely that the absence of one enhancer can be compensated under certain conditions, for example, upon receiving strong TCR stimulation (Feng et al., 2015).

Our study has also shown cooperative functions of CNS0 and CNS3 in stable maintenance of Foxp3 expression in Treg cells.

(G and H) Stat5 and H3K27ac ChIP-seq and ATAC-seq of peripheral Treg cells collected from pooled peripheral LNs and spleens of WT or CNS-deficient mice. Peak tracks (G) and quantitative analysis of H3K27ac ChIP-seq tag density of indicated regions (a to g and CNS0, CNS1, CNS2, and CNS3) (H) are shown. Data are from independently performed two (Stat5 ChIP-seq and ATAC-seq) or three (H3K27ac ChIP-seq) experiments or from previous publication (Kitagawa et al., 2017). Data show means with SDs of three biological replicates.

The percentage values were determined using flow cytometry. Graphs show means with SDs. *$p < 0.05$, **$p < 0.01$, ***$p < 0.001$, and n.s., not significant (one-way ANOVA followed by Tukey's multiple-comparison test in A, D, and E and two-way ANOVA followed by Tukey's multiple-comparison test in F). Also see Figure S6 and Data S4.

Although the roles of CNS2 in maintaining Foxp3 expression have been well documented (Feng et al., 2014; Li et al., 2014), the loss of CNS0 and/or CNS3 did not influence Stat5 binding, chromatin accessibility, or CpG hypomethylation status at CNS2, despite exhibiting decreased stability of Foxp3 expression in both *in vitro* and *in vivo* settings. However, deletion of CNS0 and CNS3 reduced the overall activity of the enhancer cluster at the *Foxp3* locus, suggesting that CNS0 and CNS3 are required to maintain the integrity of the enhancer function throughout the *Foxp3* locus. Moreover, several nuclear factors that displayed clear ChIP enrichment at CNS0 lacked compatible DNA binding motifs. It is thus likely that CNS0 and CNS3 serve as the key units of enhancer cluster by bringing together individual enhancers and the *Foxp3* promoter in three-dimensional chromatin space and providing a platform for multiple TF complexes to ensure stable control of Foxp3 expression.

A substantial number of reports have proposed factors required for Treg cell differentiation and maintenance (Burchill et al., 2008; Chen and Konkel, 2015; Mahmud et al., 2014; Moran et al., 2011; Ruan et al., 2009; Savage et al., 2020). The present study furthers these findings by the perturbation of specific non-coding regulatory elements at the enhancer resolution, demonstrating how thymic Treg cell differentiation and peripheral maintenance of Foxp3 expression are controlled by epigenetic alterations. We anticipate that recent innovations in assays such as single-cell ATAC-seq and ChIP-seq will hopefully offer additional insight on Foxp3 enhancer regulation. Moreover, other methods such as CRISPR-mediated disruption of specific enhancer sequence motifs (e.g., the Stat5 motif in CNS0) will enable profiling of enhancer function at TF resolution (Mikami et al., 2020). Together, these methods will enable systematic characterization of functional regulatory elements within the Treg cell-specific enhancers to provide better understanding of how self-tolerance is established and maintained.

Limitations of study

Although we have demonstrated the cooperative and non-redundant roles of CNS0 and CNS3 in Treg cell lineage commitment, we recognize that further work is necessary to mechanistically delineate how these two enhancers become epigenetically primed and physically accessible. In particular, the putative function of several protein species that bind to CNS0 and/or CNS3 identified by our *in silico* analyses and ChIP-seq experiments require further investigation. In addition, with the demonstration by us and Dikiy et al. (2021) (this issue of *Immunity*) of the contribution of CNS0 to IL-2 responsiveness in Foxp3 gene activation, it needs to be determined how IL-2 plays a role in CNS3-mediated Foxp3 expression in Treg-precursor cells remains. Although this study has focused solely on the individual and synergistic contributions of CNS0 and CNS3 in thymic Treg cell development, we acknowledge that other Foxp3 enhancer constituents and enhancer combinations may further reveal novel phenotypes and warrant further study.

STAR★METHODS

Detailed methods are provided in the online version of this paper and include the following:

SUPPLEMENTAL INFORMATION

Supplemental information can be found online at https://doi.org/10.1016/j.immuni.2021.04.005.

ACKNOWLEDGMENTS

We thank M. Matsuura, S. Akahori, H. Yasutomi, Y. Li, R. Takeda, T. Nagai, M. Zaizen, Z. Ci, and R. Ishii for their technical assistance. We would like to thank S. Hori for providing Foxp3-hCD2/CD52 mice. The bioinformatics analyses were conducted using the facility at the Genome Information Research Center of the Research Institute for Microbial Diseases, Osaka University, and the core facility of Graduate School of BioStudies, Kyoto University. This work was supported by a Japan Society for the Promotion of Science (JSPS) grant-in-aid for JSPS Fellows (16J03628 to R.K.), a Grant-in-Aid for Young Scientists (20K16279 to R.K.), a JSPS Grant-in-Aid for Specially Promoted Research (16H06295 to S.S.), Core Research for Evolutional Science and Technology (CREST; to S.S.), the Agency for Medical Research and Development (AMED) (JP 19gm0010005 to S.S.), and Leading Advanced Projects for Medical Innovation (LEAP; to S.S.).

AUTHOR CONTRIBUTIONS

R.K. and Y.K. designed the project, performed the experiments, and wrote the manuscript with contributions from all authors. K.Y.C. designed and performed HiChIP experiments and data analysis and wrote the manuscript. M.A. performed some parts of next-generation sequencing (NGS) experiments, data analysis, and DNA methylation analysis. D.O. performed cytokine profiling and phenotypical examination of mice. Y.N. performed DNA sequencing operations in NGS and DNA methylation analysis. K.Y. examined tissue pathology of mice. M.O. established the auto-antibody ELISA system and provided critical materials. N.M. performed part of the DNA methylation analysis. C.A.L. provided intellectual discussion on HiChIP experiments and data analysis. H.W. and G.K. established animal resources. K.H. provided animal resources, provided intellectual discussion, and designed the experiments. N.O. provided intellectual discussion and managed NGS analysis. S.S. supervised the project, designed the experiments, and wrote the manuscript. All authors reviewed the manuscript.

DECLARATION OF INTERESTS

The authors declare no competing interests.

Received: September 19, 2020
Revised: January 17, 2021
Accepted: April 8, 2021
Published: April 29, 2021

REFERENCES

Akamatsu, M., Mikami, N., Ohkura, N., Kawakami, R., Kitagawa, Y., Sugimoto, A., Hirota, K., Nakamura, N., Ujihara, S., Kurosaki, T., et al. (2019). Conversion of antigen-specific effector/memory T cells into Foxp3-expressing T_{reg} cells by inhibition of CDK8/19. Sci. Immunol. *4*, eaaw2707.

Burchill, M.A., Yang, J., Vang, K.B., Moon, J.J., Chu, H.H., Lio, C.W., Vegoe, A.L., Hsieh, C.S., Jenkins, M.K., and Farrar, M.A. (2008). Linked T cell receptor and cytokine signaling govern the development of the regulatory T cell repertoire. Immunity *28*, 112–121.

Chen, W., and Konkel, J.E. (2015). Development of thymic Foxp3(+) regulatory T cells: TGF-β matters. Eur. J. Immunol. *45*, 958–965.

Corces, M.R., Trevino, A.E., Hamilton, E.G., Greenside, P.G., Sinnott-Armstrong, N.A., Vesuna, S., Satpathy, A.T., Rubin, A.J., Montine, K.S., Wu, B., et al. (2017). An improved ATAC-seq protocol reduces background and enables interrogation of frozen tissues. Nat. Methods *14*, 959–962.

Dikiy, S., Li, J., Bai, L., Jiang, M., Janke, L., Zong, X., Hao, X., Hoyos, B., Wang, Z.-M., Xu, B., et al. (2021). A distal Foxp3 enhancer enables interleukin-2 dependent thymic Treg cell lineage commitment for robust immune tolerance. Immunity *54*. Published online April 9, 2021. https://doi.org/10.1016/j.immuni.2021.03.020.

Feng, J., Liu, T., Qin, B., Zhang, Y., and Liu, X.S. (2012). Identifying ChIP-seq enrichment using MACS. Nat. Protoc. *7*, 1728–1740.

Feng, Y., Arvey, A., Chinen, T., van der Veeken, J., Gasteiger, G., and Rudensky, A.Y. (2014). Control of the inheritance of regulatory T cell identity by a cis element in the Foxp3 locus. Cell *158*, 749–763.

Feng, Y., van der Veeken, J., Shugay, M., Putintseva, E.V., Osmanbeyoglu, H.U., Dikiy, S., Hoyos, B.E., Moltedo, B., Hemmers, S., Treuting, P., et al. (2015). A mechanism for expansion of regulatory T-cell repertoire and its role in self-tolerance. Nature *528*, 132–136.

Floess, S., Freyer, J., Siewert, C., Baron, U., Olek, S., Polansky, J., Schlawe, K., Chang, H.-D., Bopp, T., Schmitt, E., et al. (2007). Epigenetic control of the foxp3 locus in regulatory T cells. PLoS Biol. *5*, e38.

Fontenot, J.D., Gavin, M.A., and Rudensky, A.Y. (2003). Foxp3 programs the development and function of CD4+CD25+ regulatory T cells. Nat. Immunol. *4*, 330–336.

Godfrey, V.L., Wilkinson, J.E., and Russell, L.B. (1991). X-linked lymphoreticular disease in the scurfy (sf) mutant mouse. Am. J. Pathol. *138*, 1379–1387.

Heinz, S., Benner, C., Spann, N., Bertolino, E., Lin, Y.C., Laslo, P., Cheng, J.X., Murre, C., Singh, H., and Glass, C.K. (2010). Simple combinations of lineage-determining transcription factors prime cis-regulatory elements required for macrophage and B cell identities. Mol. Cell *38*, 576–589.

Hori, S., Nomura, T., and Sakaguchi, S. (2003). Control of regulatory T cell development by the transcription factor Foxp3. Science *299*, 1057–1061.

Josefowicz, S.Z., Lu, L.-F., and Rudensky, A.Y. (2012a). Regulatory T cells: mechanisms of differentiation and function. Annu. Rev. Immunol. *30*, 531–564.

Josefowicz, S.Z., Niec, R.E., Kim, H.Y., Treuting, P., Chinen, T., Zheng, Y., Umetsu, D.T., and Rudensky, A.Y. (2012b). Extrathymically generated regulatory T cells control mucosal TH2 inflammation. Nature *482*, 395–399.

Kim, H.P., and Leonard, W.J. (2007). CREB/ATF-dependent T cell receptor-induced FoxP3 gene expression: a role for DNA methylation. J. Exp. Med. *204*, 1543–1551.

Kim, J.M., Rasmussen, J.P., and Rudensky, A.Y. (2007). Regulatory T cells prevent catastrophic autoimmunity throughout the lifespan of mice. Nat. Immunol. *8*, 191–197.

Kitagawa, Y., Ohkura, N., Kidani, Y., Vandenbon, A., Hirota, K., Kawakami, R., Yasuda, K., Motooka, D., Nakamura, S., Kondo, M., et al. (2017). Guidance of regulatory T cell development by Satb1-dependent super-enhancer establishment. Nat. Immunol. *18*, 173–183.

Komatsu, N., Mariotti-Ferrandiz, M.E., Wang, Y., Malissen, B., Waldmann, H., and Hori, S. (2009). Heterogeneity of natural Foxp3+ T cells: a committed regulatory T-cell lineage and an uncommitted minor population retaining plasticity. Proc. Natl. Acad. Sci. U S A *106*, 1903–1908.

Lahl, K., Loddenkemper, C., Drouin, C., Freyer, J., Arnason, J., Eberl, G., Hamann, A., Wagner, H., Huehn, J., and Sparwasser, T. (2007). Selective depletion of Foxp3+ regulatory T cells induces a scurfy-like disease. J. Exp. Med. *204*, 57–63.

Langmead, B., and Salzberg, S.L. (2012). Fast gapped-read alignment with Bowtie 2. Nat. Methods *9*, 357–359.

Lareau, C.A., and Aryee, M.J. (2018). hichipper: a preprocessing pipeline for calling DNA loops from HiChIP data. Nat. Methods *15*, 155–156.

Li, H., Handsaker, B., Wysoker, A., Fennell, T., Ruan, J., Homer, N., Marth, G., Abecasis, G., and Durbin, R.; 1000 Genome Project Data Processing Subgroup (2009). The Sequence Alignment/Map format and SAMtools. Bioinformatics *25*, 2078–2079.

Li, X., Liang, Y., LeBlanc, M., Benner, C., and Zheng, Y. (2014). Function of a Foxp3 cis-element in protecting regulatory T cell identity. Cell *158*, 734–748.

Lio, C.W.J., and Hsieh, C.S. (2008). A two-step process for thymic regulatory T cell development. Immunity *28*, 100–111.

Loo, C.S., Gatchalian, J., Liang, Y., Leblanc, M., Xie, M., Ho, J., Venkatraghavan, B., Hargreaves, D.C., and Zheng, Y. (2020). A genome-wide CRISPR screen reveals a role for the non-canonical nucleosome-remodeling BAF complex in Foxp3 expression and regulatory T cell function. Immunity *53*, 143–157.e8.

Mahmud, S.A., Manlove, L.S., Schmitz, H.M., Xing, Y., Wang, Y., Owen, D.L., Schenkel, J.M., Boomer, J.S., Green, J.M., Yagita, H., et al. (2014). Costimulation via the tumor-necrosis factor receptor superfamily couples TCR signal strength to the thymic differentiation of regulatory T cells. Nat. Immunol. *15*, 473–481.

Mikami, N., Kawakami, R., Chen, K.Y., Sugimoto, A., Ohkura, N., and Sakaguchi, S. (2020). Epigenetic conversion of conventional T cells into regulatory T cells by CD28 signal deprivation. Proc. Natl. Acad. Sci. U S A *117*, 12258–12268.

Moran, A.E., Holzapfel, K.L., Xing, Y., Cunningham, N.R., Maltzman, J.S., Punt, J., and Hogquist, K.A. (2011). T cell receptor signal strength in Treg and iNKT cell development demonstrated by a novel fluorescent reporter mouse. J. Exp. Med. *208*, 1279–1289.

Morikawa, H., Ohkura, N., Vandenbon, A., Itoh, M., Nagao-Sato, S., Kawaji, H., Lassmann, T., Carninci, P., Hayashizaki, Y., Forrest, A.R.R., et al.; FANTOM Consortium (2014). Differential roles of epigenetic changes and Foxp3 expression in regulatory T cell-specific transcriptional regulation. Proc. Natl. Acad. Sci. USA *111*, 5289–5294.

Mumbach, M.R., Rubin, A.J., Flynn, R.A., Dai, C., Khavari, P.A., Greenleaf, W.J., and Chang, H.Y. (2016). HiChIP: efficient and sensitive analysis of protein-directed genome architecture. Nat. Methods *13*, 919–922.

Mumbach, M.R., Satpathy, A.T., Boyle, E.A., Dai, C., Gowen, B.G., Cho, S.W., Nguyen, M.L., Rubin, A.J., Granja, J.M., Kazane, K.R., et al. (2017). Enhancer connectome in primary human cells identifies target genes of disease-associated DNA elements. Nat. Genet. *49*, 1602–1612.

Ohkura, N., and Sakaguchi, S. (2020). Transcriptional and epigenetic basis of Treg cell development and function: its genetic anomalies or variations in autoimmune diseases. Cell Res. *30*, 465–474.

Ohkura, N., Hamaguchi, M., Morikawa, H., Sugimura, K., Tanaka, A., Ito, Y., Osaki, M., Tanaka, Y., Yamashita, R., Nakano, N., et al. (2012). T cell receptor stimulation-induced epigenetic changes and Foxp3 expression are independent and complementary events required for Treg cell development. Immunity *37*, 785–799.

Placek, K., Hu, G., Cui, K., Zhang, D., Ding, Y., Lee, J.E., Jang, Y., Wang, C., Konkel, J.E., Song, J., et al. (2017). MLL4 prepares the enhancer landscape for Foxp3 induction via chromatin looping. Nat. Immunol. *18*, 1035–1045.

Polansky, J.K., Kretschmer, K., Freyer, J., Floess, S., Garbe, A., Baron, U., Olek, S., Hamann, A., von Boehmer, H., and Huehn, J. (2008). DNA methylation controls Foxp3 gene expression. Eur. J. Immunol. *38*, 1654–1663.

Robinson, J.T., Thorvaldsdóttir, H., Winckler, W., Guttman, M., Lander, E.S., Getz, G., and Mesirov, J.P. (2011). Integrative genomics viewer. Nat. Biotechnol. *29*, 24–26.

Ruan, Q., Kameswaran, V., Tone, Y., Li, L., Liou, H.-C.C., Greene, M.I., Tone, M., and Chen, Y.H. (2009). Development of Foxp3(+) regulatory t cells is driven by the c-Rel enhanceosome. Immunity *31*, 932–940.

Sakaguchi, S., and Sakaguchi, N. (1989). Organ-specific autoimmune disease induced in mice by elimination of T cell subsets. V. Neonatal administration of cyclosporin A causes autoimmune disease. J. Immunol. *142*, 471–480.

Sakaguchi, S., Sakaguchi, N., Asano, M., Itoh, M., and Toda, M. (1995). Immunologic self-tolerance maintained by activated T cells expressing IL-2 receptor alpha-chains (CD25). Breakdown of a single mechanism of self-tolerance causes various autoimmune diseases. J. Immunol. *155*, 1151–1164.

Sakaguchi, S., Yamaguchi, T., Nomura, T., and Ono, M. (2008). Regulatory T cells and immune tolerance. Cell *133*, 775–787.

Samstein, R.M., Arvey, A., Josefowicz, S.Z., Peng, X., Reynolds, A., Sandstrom, R., Neph, S., Sabo, P., Kim, J.M., Liao, W., et al. (2012). Foxp3 exploits a pre-existent enhancer landscape for regulatory T cell lineage specification. Cell *151*, 153–166.

Savage, P.A., Klawon, D.E.J., and Miller, C.H. (2020). Regulatory T cell development. Annu. Rev. Immunol. *38*, 421–453.

Schmidl, C., Rendeiro, A.F., Sheffield, N.C., and Bock, C. (2015). ChIPmentation: fast, robust, low-input ChIP-seq for histones and transcription factors. Nat. Methods *12*, 963–965.

Servant, N., Varoquaux, N., Lajoie, B.R., Viara, E., Chen, C.J., Vert, J.P., Heard, E., Dekker, J., and Barillot, E. (2015). HiC-Pro: an optimized and flexible pipeline for Hi-C data processing. Genome Biol. *16*, 259.

Tone, Y., Furuuchi, K., Kojima, Y., Tykocinski, M.L., Greene, M.I., and Tone, M. (2008). Smad3 and NFAT cooperate to induce Foxp3 expression through its enhancer. Nat. Immunol. *9*, 194–202.

Wildin, R.S., Ramsdell, F., Peake, J., Faravelli, F., Casanova, J.L., Buist, N., Levy-Lahad, E., Mazzella, M., Goulet, O., Perroni, L., et al. (2001). X-linked neonatal diabetes mellitus, enteropathy and endocrinopathy syndrome is the human equivalent of mouse scurfy. Nat. Genet. *27*, 18–20.

Yoshida, H., Lareau, C.A., Ramirez, R.N., Rose, S.A., Maier, B., Wroblewska, A., Desland, F., Chudnovskiy, A., Mortha, A., Dominguez, C., et al.; Immunological Genome Project (2019). The cis-regulatory atlas of the mouse immune system. Cell *176*, 897–912.e20.

Zheng, Y., Josefowicz, S., Chaudhry, A., Peng, X.P., Forbush, K., and Rudensky, A.Y. (2010). Role of conserved non-coding DNA elements in the Foxp3 gene in regulatory T-cell fate. Nature *463*, 808–812.

Zhou, X., Lowdon, R.F., Li, D., Lawson, H.A., Madden, P.A.F., Costello, J.F., and Wang, T. (2013). Exploring long-range genome interactions using the WashU Epigenome Browser. Nat. Methods *10*, 375–376.

STAR★METHODS

KEY RESOURCES TABLE

REAGENT or RESOURCE	SOURCE	IDENTIFIER
Antibodies		
Monoclonal anti-human CD2 (clone RPA-2.10)	BioLegend	Cat #300214 RRID: AB_10895925
Monoclonal anti-human/mouse CD44 (clone IM7)	BD	Cat #103039 RRID: AB_10895752
Monoclonal Rat anti-IgG antibody (clone RTK2071)	BioLegend	Cat #400414 RRID:AB_326520
Monoclonal anti-mouse IL-2 antibody (clone JES6-1A12)	BioLegend	Cat #503705 RRID: AB_11150768
Monoclonal anti-mouse B220 (clone RA3-6B2)	BD	Cat #51-01122J: RRID:AB_10053179
Monoclonal anti-mouse c-Kit/CD117 (clone2B8)	BioLegend	Cat #105808 RRID: AB_313217
Monoclonal anti-mouse CD103 (clone 2E7)	BioLegend	Cat #121414 RRID: AB_1227502
Monoclonal anti-mouse CD11b (clone M1/70)	BD	Cat #51-01712J: RRID:AB_10053179
Monoclonal anti-mouse CD11c (clone HL3)	BD	Cat #553800 RRID:AB_395059
Monoclonal anti-mouse CD152 (CTLA-4) (clone UC10-4B9)	eBioScience	Cat #17-1522-82 RRID:AB_2016700
Monoclonal anti-mouse CD16/32 (clone 2.4G2)	BD	Cat #553142 RRID:AB_394657
Monoclonal anti-mouse CD19 (clone 1D3)	BD	Cat #550992 RRID:AB_398483
Monoclonal anti-mouse CD25 (clone PC61)	BD	Cat #553866 RRID:AB_395101
Monoclonal anti-mouse CD28 (clone 37.51)	BD	Cat #553294 RRID:AB_394763
Monoclonal anti-mouse CD3ε (clone 145-2C11)	BD	Cat #553057 RRID:AB_394590
Monoclonal anti-mouse CD4 (clone RM4-5)	BioLegend	Cat #100559 RRID: AB_2562608
Monoclonal anti-mouse CD45.1 (clone A20)	BD	Cat #560580 RRID:AB_1727489
Monoclonal anti-mouse CD45.2 (clone 104)	BioLegend	Cat #109832 RRID:AB_2565511
Monoclonal anti-mouse CD62L (clone MEL-14)	BD	Cat #560513 RRID:AB_10611578
Monoclonal anti-mouse CD8a (clone 53-6.7)	BD	Cat #553036 RRID:AB_394573
Monoclonal anti-mouse CD8a (clone 2.43)	CST	Cat #72461S RRID:AB_2799823
Monoclonal anti-mouse FR4 (clone 12A5)	BD	Cat #560318 RRID:AB_1645227
Monoclonal anti-mouse GITR (clone DTA-1)	BD	Cat #558140 RRID:AB_647252
Monoclonal anti-mouse Helios (clone 22F6)	BioLegend	Cat #137218 RRID:AB_10660750
Monoclonal anti-mouse I-A/I-E (clone M5/114.15.2)	Invitrogen	Cat #12-5321-83 RRID:AB_465928
Monoclonal anti-mouse ICOS (clone C398.4A)	eBioScience	Cat #17-9949-82 RRID:AB_11149880
Monoclonal anti-mouse IFN-γ (clone XMG1.2)	eBioScience	Cat #25-7311-82 RRID:AB_469680
Monoclonal anti-mouse IL-17A (clone TC11-18H10.1)	BioLegend	Cat #506903 RRID:AB_315463
Monoclonal anti-mouse IL-4 (clone 11B11)	BD	Cat #554435 RRID:AB_395391
Monoclonal anti-human/mouse Ki67 (clone B56)	BD	Cat #556027 RRID:AB_2266296
Monoclonal anti-mouse Klrg1 (clone 2F1)	eBioScience	Cat #25-5893-80 RRID:AB_1518769
Monoclonal anti-mouse Ly6C/G (clone RB6-8C5)	BD	Cat #553124 RRID:AB_394640

(*Continued on next page*)

Continued

REAGENT or RESOURCE	SOURCE	IDENTIFIER
Monoclonal anti-mouse CD304 (Neuropilin-1, clone 3DS304M)	eBioscience	Cat #48-3041-80 RRID:AB_2574050
Monoclonal anti-mouse Ox40 (clone OX-86)	eBioscience	Cat #119409 RRID:AB_2272150
Monoclonal anti-mouse TCR-beta (clone H57-597)	BioLegend	Cat #109229 RRID:AB_10933263
Monoclonal anti-mouse Ter119 (clone TER-119)	BioLegend	Cat #116204 RRID:AB_313705
Monoclonal anti-mouse Tigit (clone 1G9)	BioLegend	Cat #142103 RRID:AB_10895760
Monoclonal anti-mouse Zap70 (clone1E7.2)	eBioscience	Cat #12-6695-80 RRID:AB_466140
Monoclonal anti-mouse/rat FoxP3 (clone FJK-16 s)	eBioscience	Cat #17-5773-82 RRID:AB_469457
Monoclonal anti-mouse CD8 (clone 53-6.7)	BioLegend	Cat #100704 RRID:AB_312743
Monoclonal anti-mouse CD25 (clone PC61.5)	eBioScience	Cat #17-0251-82 RRID:AB_469366
Monoclonal anti-mouse CD4 (clone RM4-4)	BioLegend	Cat #116010 RRID:AB_2561504
Monoclonal anti-human CD2 (clone RPA-2.10)	BD	Cat #562667 RRID:AB_2737708
Monoclonal anti-mouse c-Kit/CD117 (clone2B8)	BioLegend	Cat #105816 RRID: AB_493472
Monoclonal anti-mouse CD3ε (clone 145-2C11)	BD	Cat #553060 RRID:AB_394593
Monoclonal anti-mouse CD3ε (clone 145-2C11)	BioLegend	Cat #100306 RRID: AB_312671
Monoclonal anti-mouse CD3ε (clone 145-2C11)	eBioScience	Cat #12-0031-82 RRID:AB_465496
Monoclonal anti-mouse CD19 (clone 6D5))	BioLegend	Cat #115537 RRID: AB_10895761
Monoclonal anti-mouse CD24 (clone M1/69)	BioLegend	Cat #101826 RRID: AB_2563508
Monoclonal anti-mouse/rat FoxP3 (clone FJK-16 s)	eBioscience	Ca t#53-5773-82 RRID:AB_763537
Polyclonal Rabbit anti-H3K27ac	GeneTex	Cat #GTX60815 RRID: Not Available
Polyclonal Rabbit anti-H3K27me3	Merck Millipore	Cat #07-449 RRID:AB_310624
Polyclonal Rabbit anti-H3K4me1	Active Motif	Cat #39297 RRID:AB_2615075
Monoclonal Mouse anti-H3K4me3 (clone mAbcam1012)	Abcam	Cat #ab1012 RRID:AB_442796
Monoclonal Rabbit anti-STAT5a (clone E289)	Abcam	Cat #ab32043 RRID:AB_778107
Monoclonal Rabbit anti-c-Fos (clone 9F6)	CST	Cat #2250 RRID:AB_2247211
Monoclonal Mouse anti-Rela/p65 (clone F-6)	SantaCurz	Cat #sc8008 RRID:AB_628017
Monoclonal Rabbit anti-NFAT1 (clone D43B1)	CST	Cat #5861 RRID:AB_10834808
Monoclonal Rabbit anti TET2 (mouse specific) (clone D9K3E)	CST	Cat #92529 RRID:AB_2800188
Monoclonal Mouse anti-Ep300 (clone 3G230)	Abcam	Cat #ab14984 RRID:AB_301550
Polyclonal Rabbit anti-CTCF	Diagenode	Cat #C15410210-50 RRID:AB_2753160
Monoclonal Rabbit anti-H3K27ac (clone EP16602)	Abcam	Cat #ab177178 RRID:AB_2828007
Polyclonal Rabbit IgG	Abcam	Cat #ab171870 RRID:AB_2687657
Goat Anti-mouse IgG HRP-conjugated	Sigma Aldrich	Cat #A4416-5ML RRID:AB_258167
Chemicals, peptides, and recombinant proteins		
Streptavidin-APC	BD	Cat #554067 RRID:AB_10050396
Streptavidin-BV421	BioLegend	Cat #405225 RRID: Not Available
Streptavidin-PE-cy7	BD	Cat #557598 RRID: Not Available
recombinant human IL-2 (IMUNACE35)	SHIONOGI & CO., LTD.	N/A
recombinant mouse TNF-alpha	R&D	Cat #410-MT-010
recombinant human TGF-beta1	PeproTech	Cat #AF-100-21C

(*Continued on next page*)

Continued

REAGENT or RESOURCE	SOURCE	IDENTIFIER
Critical commercial assays		
LIVE/DEAD Fixable Near-IR Dead Cell Stain Kit	ThermoFisherScientific	Cat #L34975
Anti-PE MicroBeads	Miltenyi Biotec	Cat #130-048-801
Streptavidin MicroBeads	Miltenyi Biotec	Cat #130-048-101
BD Imag Mouse CD4 T Lymphocyte Enrichment Set	BD	Cat #558131
Illumina Tagment DNA Enzyme and Buffer Kit	Illumina	Cat #20034211
iDeal ChIP-seq kit for Transcription Factors	Diagenode	Cat #C01010055
Dynabeads Mouse T-Activator CD3/CD28	ThermoFisherScientific	Cat #11452D
BD Cytokine Beads Array Flex Set TNF	BD	Cat #558299
BD Cytokine Beads Array Flex Set IL-5	BD	Cat #558302
BD Cytokine Beads Array Flex Set IL-6	BD	Cat #558301
Phorbol 12-myristate 13-acetate	Sigma	Cat #P1585
Ionomycin	Sigma	Cat #I0634
Brefeldin A	Merck Millipore	Cat #203729
Formaldehyde	ThermoFisherScientific	Cat #28906
Formaldehyde	Sigma Aldrich	Cat #F8775
LBIS anti-dsDNA mouse ELISA Kit	Fujifilm-Wako-Shibayagi inc.	Cat #AKRDD-061
ProteoExtract Subcellular Proteome Extraction Kit	Merck Millipore	Cat #539790
DAB substrate	BD	Cat #555214
MethylEasy Xceed Rapid DNA Bisulfite Modification Kit	Human Genetic Signatures	Cat #ME002
Ion Plus Fragment Library Kit	ThermoFisherScientific	Cat #4471252
NEBNext Ultra II DNA Library Prep Kit for Illumina	Illumina	Cat #E7645
Dynabeads MyOne Streptavidin C1	ThermoFisherScientific	Cat #65001
KAPA HiFi DNA Polymerase	KAPA Biosystems	Cat #7958838001
Deposited data		
HiChIP raw sequence data	This paper	DRA010814
ChIP-seq, ATAC-seq raw sequence data	This paper	DRA011637
ChIP-seq data	Kitagawa et al., 2017	DRP003376
Experimental models: organisms/strains		
Mouse: C57BL/6J	CLEA Japan	
Mouse: Foxp3-IRES-DTR-GFP KI (FDG)	Kim et al., 2007	
Mouse: Foxp3-IRES-hCD2/hCD52 (Foxp3-hCD2)	(Komatsu et al., 2009)	
Mouse: CNS0-deficient/FDG	This study	
Mouse: CNS3-deficient/FDG	This study	
Mouse: CNS0and3-double deficient/FDG	This study	
Mouse: CNS0-deficient/Foxp3-hCD2	This study	
Mouse: CNS3-deficient/ Foxp3-hCD2	This study	
Mouse: Foxp3-IRES-DTR-GFP BAC-Tg (DEREG)	Lahl et al., 2007	
Oligonucleotides		
Foxp3-CNS0 gRNA-F; 5′-TCTTAT TCCATCGGCAGTTG(TGG)-3′	This paper	N/A
Foxp3-CNS0 gRNA-R; 5′-GCTTCA GAATCGTTGGCCAC(AGG)-3′	This paper	N/A

(*Continued on next page*)

Continued

REAGENT or RESOURCE	SOURCE	IDENTIFIER
Foxp3-CNS3 gRNA-F; 5′-CAGTAAA GGTCGACACCTAT(AGG)-3′	This paper	N/A
Foxp3-CNS3 gRNA-R; 5′-TAAGGT CTCCTATCGGGATG(AGG)-3′	This paper	N/A
CNS0KO genotyping forward primer 5′-ATATACACAAGTGGACGGTA-3′	This paper	N/A
CNS0KO genotyping reverse primer 5′-GGTCCTGCAAGCTAGGGAAA-3′	This paper	N/A
CNS3KO genotyping forward primer 5′-AAGGTCGGGACCTGCGAAGT-3′	This paper	N/A
CNS3KO genotyping reverse primer 5′-GAGCTGGCCCCAACACTGTT-3′	This paper	N/A
PCR primer for bisulfite sequence	Ohkura et al., 2012	N/A
Software and algorithms		
Bowtie2	(Langmead and Salzberg, 2012)	http://bowtie-bio.sourceforge.net/bowtie2/index.shtml
Samtools	(Li et al., 2009)	http://samtools.sourceforge.net/
Trim-Galore	Babraham Bioinformatics	https://www.bioinformatics.babraham.ac.uk/projects/trim_galore/
Fastx-tool kit	Hannon Lab	http://hannonlab.cshl.edu/fastx_toolkit/
MACS2	Feng et al., 2012	https://github.com/macs3-project/MACS/
homer	Heinz et al., 2010	http://homer.ucsd.edu/homer/
R	The R Foundation	https://www.r-project.org/
HiC-Pro pipeline	Mumbach et al., 2017; Servant et al., 2015	
hichipper pipeline	Lareau and Aryee, 2018; Yoshida et al., 2019	
WashU Epigenome Browser	Roadmap Epigenomics Project and the ENCODE project. (Zhou et al., 2013)	https://epigenomegateway.wustl.edu/
IGV genome browser	Broad Institute (Robinson et al., 2011)	https://software.broadinstitute.org/software/igv/
Flow Jo_v10	Flowjo	https://www.flowjo.com/
GraphPad Prism 7	GraphPad Software	https://www.graphpad.com/scientific-software/prism/
Picard	Broad Institute	https://broadinstitute.github.io/picard/
Bedtools	Quinlan Lab	https://bedtools.readthedocs.io/en/latest/
Other		
FACSCanto	BD	N/A
FACSCelesta	BD	N/A
FACSAriaII	BD	N/A
IonS5 sequencer system	ThermoFisherScientific	N/A

RESOURCE AVAILABILITY

Lead contact

Further information and requests for resources and reagents should be directed to and will be fulfilled by the Lead Contact, Shimon Sakaguchi (shimon@ifrec.osaka-u.ac.jp).

Materials availability

Mouse lines generated in this study will be deposited upon request.

Data and code availability

All data discussed in this paper are included in this article and online supplemental materials. The accession number for the HiChIP data reported in this paper is DNA Data Bank of Japan Sequence Read Archive, DDBJ: DRA010814. The accession number for the ChIP-seq and ATAC-seq data reported in this paper is DDBJ: DRA011637, or National Center for Biotechnology Information (NCBI) Sequence Read Archive, SRA: DRP003376 (Kitagawa et al., 2017).

EXPERIMENTAL MODEL AND SUBJECT DETAILS

Mice

All animals used in this study were maintained in specific pathogen-free condition. All experiments using animals were performed following the guidelines on animal welfare of Osaka University and Kyoto University.

C57BL/6 mice were purchased from CLEA Japan inc. C57BL/6 (CD45.1) congenic mice were bred in our animal facility. Foxp3-IRES-DTR-GFP mice (FDG), Foxp3-IRES-hCD2-hCD52 mice (Foxp3-hCD2), BAC-transgenic Foxp3 promoter-DTR-GFP mice (DEREG), *Rag2*-deficient mice were previously described (Hori et al., 2003; Kim et al., 2007; Komatsu et al., 2009; Lahl et al., 2007).

Thymocyte preparation was performed using age-matched, 3 to 6-week-old male mice. Other experiments were performed using 8 to 12-week-old male mice unless specially mentioned otherwise. CRISPR/Cas9-mediated targeting on Foxp3-CNS0 and/or -CNS3 was performed using C57BL/6 FDG or Foxp3-hCD2-hCD52 mice. For CNS0 and CNS3-double deficient mice generation, we targeted CNS3 using oocytes of CNS0-deficient mice. Mice were used for experiments after backcrossed with wild-type mice at least three times in order to minimize the effect of non-specific targeting by CRISPR/Cas9 system. The sequences of guide RNAs are described below (target sequence and (PAM)); Foxp3-CNS0-A; TCTTATTCCATCGGCAGTTG(TGG), Foxp3-CNS0-B; GCTTCAGAATCGTTGGCCAC(AGG), Foxp3-CNS3-A; CAGTAAAGGTCGACACCTAT(AGG), Foxp3-CNS3-B; TAAGGTCTCCTATCGGGATG(AGG).

METHOD DETAILS

Antibodies and reagents

Antibodies, reagents and critical commercial assays used in this study are listed in Key resource table.

Flow cytometry analysis and cell sorting

For cell surface staining, prepared cell suspension was incubated with anti-CD16/32 Fc-Block (BioLegend) and fluorescence-conjugated antibody cocktail in Flow cytometry buffer (2% FCS and 1mM EDTA in PBS or RPMI1640) for 20-40 min on ice. Dead cell staining (LifeTechnologies) was added if necessary. For intracellular staining, we used Foxp3 staining buffer kit (eBioScience) following manufacturer's instruction. Flow cytometry analysis was performed using FACSCantoII or FACSCelesta (BD). Cell sorting was performed using FACSAriaII (BD). For cell sorting of peripheral cells, we pooled the cells of lymph nodes (inguinal, axilla, submandibular) and spleen followed by pre-enrichment of $CD4^+$ cells using BDiMag CD4 enrichment kit (BD). For cell sorting of thymocytes, DP, CD8SP and erythroid cells were eliminated by anti-CD8-biotin Ab and anti-Ter119-biotin Ab with MACS LD depletion system (Millteny Biotech) according to the manufacturer's instruction.

Gating strategies for the cell fractions used in this study are described below;

thymic immature CD4 single positive cells (ImCD4SP); $CD4^+CD8^-CD25^-$Foxp3-eGFP (or hCD2)$^-CD24^{hi}$

thymic CD25 single positive cells (Precursor 1); $CD4^+CD8^-CD25^+$Foxp3-eGFP (or hCD2)$^-$

thymic Foxp3 single positive cells (Precursor 2); $CD4^+CD8^-CD25^-$Foxp3-eGFP (or hCD2)$^+$

thymic Treg cells (tTreg); $CD4^+CD8^-CD25^+$Foxp3-eGFP (or hCD2)$^+$

peripheral naive T cells (Tnaive); $CD4^+CD25^-$Foxp3-eGFP (or hCD2)$^-CD44^{low}$ $CD62L^{hi}$

peripheral Treg cells; $CD4^+CD25^+$Foxp3-eGFP (or hCD2)$^+$

splenic B cells; $CD3^{neg}CD19^+MHCII^+$

Lin^-c-kit^+ bone marrow progenitor cells (Lin^- BM progenitors); Lineage marker$^-$ (CD11b, CD11c, Ter119, Ly6C/G, B220, CD3, CD4, CD8, CD19) c-kit^{hi}

thymic DN2; $CD45^+CD4^-CD8^-$c-$kit^{hi}CD25^{hi}$

thymic DN3; $CD45^+CD4^-CD8^-$c-kit^-CD25^{hi}

thymic double positive (DP), $CD4^+CD8^+$

thymic early-phase $CD3^{neg}$ DP; $CD4^+CD8^+$ TCR-β^-CD3^-

thymic late-phase $CD3^+$ DP; $CD4^+CD8^+$ TCR-β^+CD3^+

thymic CD8 single positive cells (CD8SP); $CD4^-CD8^+$

Cell culture, Treg cell induction and Treg cell stability assay *in vitro*

Purified T cells (purity > 95%) were cultured *in vitro* in the 37°C, 5% CO_2 incubator using RPMI1640 culture medium supplemented with 10% FCS (v/v), 60 μg/ml penicillin G, 100 μg/ml streptomycin, 0.1 mM 2-mercaptoethanol. For iTreg cell induction from peripheral Tnaive cells, sorted 1×10^5 Tnaive cells ($CD4^+CD25^-$Foxp3-eGFP$^-CD62L^{hi}CD44^{low}$) were stimulated in a 96-well plate using plate-coated anti-CD3 antibody with soluble anti-CD28 antibody in the presence of 50 U/ml IL-2 and 2.5 ng/ml TGF-β. The

concentration of antibodies is indicated in the figure legends. For tTreg cell differentiation assay or Treg cell stability analysis of thymic or peripheral Treg cells *in vitro*, 2×10^4 of cells were stimulated with 100U/ml IL-2, with or without Dynabeads mouse CD3/CD28 T cell stimulator (GIBCO) for consecutive 3 - 6 days. Stimulated cells were analyzed by flow cytometry after removing Dynabeads.

Treg cell stability assay *in vivo*

1.5×10^5 of $CD4^+CD25^-CD45RB^{hi}$ Tnaive cells from $CD45.1^+$ C57BL/6 and 1.5×10^5 of $CD4^+CD25^+GFP^+$ Treg cells from $CD45.2^+$ wild-type or CNS-deficient FDG mice were mixed and intravenously transferred into *Rag2*-deficient recipients. Body weight of recipients was measured once a week up to day 56. Reduction of body weight was assessed by the ratio of body weight to day 0. At day 56, all mice were sacrificed and subjected to flow cytometric analyses, inspection of histology, and CpG DNA methylation analysis by bisulfite-sequencing.

Mixed bone marrow chimeric transfer

Bone marrow cells were prepared from femur and tibia of $CD45.1^+$ wild-type C57BL/6 or $CD45.2^+$ indicated gene-edited mice, using 23G needle and syringe. Red blood cells and $CD3^+$ T cells were removed using Red Blood Cell Lysis Buffer (Sigma) and MACS negative selection system (Millteny) following manufacturer's protocol. 2×10^6 of $CD45.1^+$ and $CD45.2^+$ bone marrow cells were mixed in PBS suspension followed by intravenous injection into sub-lethally irradiated (3.0 Gly) $CD45.1^+$ *Rag2*$^{-/-}$ recipients. Five weeks later, mice were sacrificed and analyzed. Gating strategy for Treg cell population analysis is followed; WT CD4SPs; $CD45.1^+CD45.2^-CD3^+CD4^+$, CNS-deficient CD4SPs; $CD45.1^-CD45.2^+CD3^+CD4^+$.

Tissue histology inspection

The scoring of tissue pathology or abnormality was examined as previously described (Kitagawa et al., 2017). Freshly-isolated tissues were immediately fixed by 10% formaldehyde. H&E staining and microscopy slide preparation was performed by the Center for Anatomical, Pathological and Forensic Medical Research, Kyoto University Graduate School of Medicine. For scoring of tissue inflammation, the following criteria were used;

Pneumonitis: 0 no pneumonitis, 1 mild inflammation, 2 intermediate inflammation, 3 severe inflammation and tissue destruction.

Gastritis: 0 no gastritis, 1 submucosal inflammation, 2 mild mucosal inflammation, 3 intermediate mucosal inflammation with destruction of gastric glands, 4 severe mucosal inflammation with loss of parietal cells.

Colitis: 0 no colitis, 1 minimal scattered mucosal inflammatory cell infiltrates, with or without minimal epithelial hyperplasia, 2 mild scattered to diffuse inflammatory cell infiltrates, 3 mild to moderate inflammatory cell infiltrates with moderate epithelial hyperplasia and mucin depletion, 4 marked inflammatory cell infiltrates that were often transmural and associated with ulceration with marked epithelial hyperplasia and mucin depletion, 5 marked transmural inflammation with severe ulceration and loss of intestinal glands.

Dermatitis: 0 no dermatitis, 1 inflammatory cell infiltration, 2 mild inflammation, 3 intermediate inflammation, 4 severe inflammation.

Cytokine expression assay

Measurement of serum cytokines (TNF, IL-6, IL-5) were performed using BD Cytometric Bead Array Flex Set following manufacturer's instruction. For intracellular staining of cytokines (IFN-γ, IL-4, IL-17), sorted cells were stimulated *in vitro* for 2.5 hours with 0.5 μg/ml of Phorbol 12-myristate 13-acetate, 0.5 μg/ml Ionomycin, and 1 μg/ml Brefeldin A. Fixation was performed using 3.7% Formaldehyde at room temperature for 20 minutes. After removal of Formaldehyde by centrifugation, permeabilization was performed using 0.1 % NP-40 at room temperature for 3 minutes. After washing cells once using PBS, intracellular staining was performed at room temperature for 30 minutes, followed by flow cytometry analysis.

Auto-antibody detection by ELISA

ELISA for anti-double stranded-DNA antibody was performed using LBIS anti-dsDNA mouse ELISA Kit (Fujifilm-Wako-Shibayagi inc.) following the manufacturer's instruction. ELISA for anti-parietal cell antibody was performed following the previously described protocol with minor modification (Sakaguchi and Sakaguchi, 1989). Briefly, BALB/c-derived gastric tissue was minced using gentleMax Dissociator (Millteny BioTech) and digested using Liberase and DNase I. After trituration of digested tissue, debris were removed by filtration using 40 μm nylon mesh filter, followed by protein extraction using ProteoExtract Subcellular Proteome Extraction Kit (Merck Millipore) following the manufacturer's instruction. For ELISA, 10 μg of Parietal cell antigen extract was loaded on Nunc MaxiSorp 96 well multiwell ELISA plate (ThermoFisher) over one night, followed by blocking using 1% BSA PBS-T buffer. Serum was incubated on the antigen-coated plate for 2 hours at room temperature. After washing out unreacted serum, plate was incubated with HRP-conjugated anti-mouse IgG (Sigma Aldrich). Detection was performed using DAB substrate (BD) and 0.1 M H_2SO_4. 450 nm was measured by multi-well plate reader iMark (BioRad).

CpG methylation analysis by bisulfite sequencing

Genome DNA was collected from 2×10^4 of cells by Phenol-chloroform extraction. 10-100 ng of DNA was subjected to bisulfite reaction using MethylEasy Xceed Rapid DNA Bisulfite Modification Kit (Human Genetic Signatures) following the manufacturer's instruction. PCR primers, conditions, and methods for DNA sequencing are previously described (Ohkura et al., 2012).

ChIP-seq

ChIP-seq experiments were performed in two ways depending on the appropriate combination of methods and antibody; as previously described with minor modification (Kitagawa et al., 2017) or using iDeal ChIP Kit for Transcription Factors (Diagenode) following the manufacture's instruction. For Stat5 ChIP-seq experiment, cells were stimulated with 100 U/ml IL-2 for 30 min at 37°C. Before Rela/p65 ChIP-seq experiment, cells were stimulated with 1 μg/ml PMA and 1 μg/ml Ionomycin for 10 min at 37°C. Other ChIP-seq experiments were performed using *ex vivo* sorted untreated cells. Sorted cells were fixed using 1% Formaldehyde (ThermoScientific) for 10 minitutes for anti-Histone ChIP or 15 minutes for anti-TF ChIP at room temperature. After nuclear extraction, chromatin lysate was fragmentated using Picoruptor (Diagenode) at 4°C before immunoprecipitation, in which Sonication versus Cooling was set to 30 s and 30 s, 7 to 10 cycles. Immunoprecipitated chromatin lysate was reverse-crosslinked at 65°C for 8 or 20 hours, followed by purification and library preparation using NGS library preparation kit for IonS5 (ThermoScientific) or NEBNext Ultra II DNA Library Prep Kit for Illumina (Illumina) according to manufacturer's instructions. Raw NGS data was produced by IonS5 sequencer system (ThermoScientific) or HiSeq2500 (Illumina).

ATAC-seq

ATAC-seq was performed as previously described with minor modifications (Corces et al., 2017). Briefly, sorted 5×10^4 target cells were lysed using 50 μl of lysis buffer (0.01% digitonin, 0.1% NP-40, 0.1% Tween 20 in resuspension buffer; 10 mM Tris-HCl pH7.5, 100 mM NaCl, 3 mM $MgCl_2$) for 3 minutes on ice. After removing lysis buffer by centrifugation, Tn5 tagmentation was performed using Illumina Tagment DNA TDE1 Enzyme and Buffer Kits (Illumina) at 37°C for 30 min, with shaking at 1000 rpm following manufacturer's instruction. After purification using DNA Clean & Concentrator-5 (Zymo Research), tagmented DNA was amplified using NEBNext High-Fidelity PCR Master Mix (New England BioLabs) with the following primers: 5′-CAAGCAGAAGACGGCATACGAGATNNNN NNNNGTCTCGTGGGCTCGGAGATGT-3′ and 5′-AATGATACGGCGACCACCGAGATCTACACNNNNNNNNTCGTCGGCAGCGTCA GATGTG-3′ (barcode sequences are indicated as NNNNNNNN). Prepared DNA libraries were size-selected (150-1000 bp) by Ampure XP (Beckman Coulter). Sequencing was performed using NextSeq500 or NovaSeq (Illumina).

Data processing and analyses of ChIP-seq and ATAC-seq data

The quality of sequence reads was confirmed using fastQC to confirm that the average of Phred score was over 20. Raw sequences were trimmed and fastx_trimmer in fastx_tool kit (Hannon Lab), using following setting; fastx_trimmer -f 1 -l 240 -i ${name}.fastq -Q33 | fastq_quality_trimmer -t 20 -l 20 -o ${name}_trimmed.fastq -Q33. For ChIP-seq analysis, sequencing reads were mapped to mm9 using Bowtie2 with default setting. Peak call was performed using MACS2 by the following command; macs2 callpeak -t ${filename}. sam -c input.sam -g mm -n SPMR_${filename} -B–nomodel–SPMR. IGV Integrated genome viewer was used for the visualization of peak or region data using group-auto scaling, auto-scaling based on *Actb* locus, or normalized to total mapped reads. For ATAC-seq analysis, sequenced reads were processed by Trim-galore 0.6.6 (Babraham Bioinformatics) to remove nextera barcode sequence and quality trimming, using following command; trim_galore–fastqc–nextera–paired R1.fastq.gz R2.fastq.gz. Trimmed sequences of which Phred score over 20 were used for downstream analysis. Processed reads were mapped to modified mm9 reference, in which mitochondrial chromosome (ChrM) was removed, using Bowtie2 with default setting. After removal of PCR duplicates using Picard (Broad institute), peak call was performed using MACS2 (Feng et al., 2012) by the following command; macs2 callpeak -t ${filename}.bam -g mm -n ${filename} -B–nomodel–shift 100–extsize 200–keep-dup all–SPMR. Tag density per 10 million mapped reads at particular regions was determined using homer annotatePeaks.pl (Heinz et al., 2010) using following option; annotatePeaks.pl regions.bed mm9 -size given -d tagdir1, tagdir2 .... > out.txt. Heatmap was described using an R package ggplot2.

HiChIP genomic interaction analysis

The HiChIP protocol was performed essentially as previously described (Mumbach et al., 2016, 2017), with the following modifications. 2.5 million cells were used per T cell subtype per replicate for H3K27ac HiChIP using antibody anti-H3K27ac antibody (ab177178). Sonication was performed using Diagenode Bioruptor Plus with the following parameters: High power setting for 5 cycles (30 s ON 30 s OFF) and then clarified by centrifugation for 15 min at 15,000 RCF at 4°C. After washing with lithium chloride, sample beads were washed twice with cold 10 mM Tris-HCl pH 8.0 to remove residual detergents and on-bead tagmentation by ChIPmentation was carried out as previously described (Schmidl et al., 2015). 1 mL of HiChIP Low salt buffer (0.1% SDS, 1% Triton X-100, 2 mM EDTA, 20 mM Tris- HCl pH 7.5, 150 mM NaCl) was added to stop the tagmentation reaction and samples were then washed twice with TE buffer. Sample beads were resuspended in 100 uL reverse crosslinking buffer (0.2 M NaCl, 50 mM Tris-HCl pH 7.5, 1 mM EDTA, 1 % SDS and 200 g/ml Proteinase K) and incubated at 65°C for overnight with shaking. Beads were removed and the supernatant was purified with ChIP DNA Clean & Concentrator (Zymo Research) and eluted in 10 μL of EB twice for a total of volume of 20 μL. 10 μL of Streptavidin C-1 beads (Thermo Fisher) were washed with Tween Wash Buffer (5 mM Tris-HCl pH 7.5, 0.5 mM EDTA, 1 M NaCl, 0.05% Tween-20) and then resuspended in 20 μL of 2X biotin binding buffer (10 mM Tris-HCl pH 7.5, 1 mM EDTA, 2 M NaCl). Beads were directly added to the eluted samples and then incubated at room temperature for 15 minutes with shaking to allow for the biotinylated DNA to bind to the beads. Beads were then placed on a magnet and washed three times with Tween Wash Buffer and incubated at 55°C for 2 min with shaking. A final wash with 10 mM Tris-HCl pH 8.0 was performed before carefully resuspending the beads in 35 μL EB buffer.

On-beads PCR was performed by adding 1.25 μL of each Nextera Ad1_noMX and Nextera Ad2.X forward and reverse primers at 10 μM, 10 μL 5X KAPA HiFi Fidelity Buffer (Roche), 1.5 μL KAPA dNTP Mix and 1 μL KAPA HiFi DNA Polymerase. The following PCR

program was performed: 72°C for 5 min, 98°C for 1 min, then cycle at 98°C for 20 s, 63°C for 30 s, and 72°C for 1 min. Cycle number determination and subsequent purification by Ampure beads was done as previously described (Mumbach et al., 2016). After size selection, libraries were quantified by qPCR and then sequenced with paired-end reads on the Illumina HiSeq 2500 or Illumina NextSeq 550.

HiChIP data processing

HiChIP libraries were aligned to the mm9 genome using the HiC-Pro pipeline as previously described (Mumbach et al., 2017; Servant et al., 2015). Aligned data was subsequently processed through the hichipper pipeline using all ImmGen ATAC consensus peaks as peak anchors for loop calling with default parameters (Lareau and Aryee, 2018; Yoshida et al., 2019). Intrachromsomal long range interactions were defined as interactions spanning over two anchor regions on the same chromosome with a minimum length of 2 Kbp and a maximum length of 2 Mbp. High-confidence loop calls along with HiC-Pro interaction heatmaps were visualized on the WashU Epigenome Browser.

QUANTIFICATION AND STATISTICAL ANALYSIS

Statistical analysis was performed using GraphPad Prism software or R package DESeq2. Data were expressed as mean ± SD with the dot plot of individual experiments. Statistical significance was estimated based on paired or unpaired Student's t test (for two group), One-way or Two-way non-repeated-measures analysis of variance (ANOVA) followed by Turkey's multiple comparison test, or Two-way ANOVA followed by Sidak's multiple comparison test, using GraphPad Prism 7. Statistical significance was marked as *$p < 0.05$, **$p < 0.01$, ***$p < 0.001$.